

7-8-2016

# Computational Fluid Dynamic analysis of Microbubble Drag Reduction Systems at High Reynolds Number

John D. Goolcharan

*Florida International University*, [jgool010@fiu.edu](mailto:jgool010@fiu.edu)

**DOI:** 10.25148/etd.FIDC000788

Follow this and additional works at: <https://digitalcommons.fiu.edu/etd>

 Part of the [Aerodynamics and Fluid Mechanics Commons](#), [Computer-Aided Engineering and Design Commons](#), and the [Other Mechanical Engineering Commons](#)

---

## Recommended Citation

Goolcharan, John D., "Computational Fluid Dynamic analysis of Microbubble Drag Reduction Systems at High Reynolds Number" (2016). *FIU Electronic Theses and Dissertations*. 2542.

<https://digitalcommons.fiu.edu/etd/2542>

This work is brought to you for free and open access by the University Graduate School at FIU Digital Commons. It has been accepted for inclusion in FIU Electronic Theses and Dissertations by an authorized administrator of FIU Digital Commons. For more information, please contact [dcc@fiu.edu](mailto:dcc@fiu.edu).

FLORIDA INTERNATIONAL UNIVERSITY

Miami, Florida

COMPUTATIONAL FLUID DYNAMIC ANALYSIS OF MICROBUBBLE DRAG  
REDUCTION

A thesis submitted in partial fulfillment of the

requirements for the degree of

MASTER OF SCIENCE

in

MECHANICAL ENGINEERING

by

John Goolcharan

2016

To: Interim Dean Ranu Jung  
College of Engineering and Computer Science

This thesis, written by John Goolcharan and entitled Computational Fluid Dynamic Analysis of Microbubble Drag Reduction, having been approved in respect to style and intellectual content, is referred to you for judgment.

We have read this dissertation and recommend that it be approved.

---

Yiding Cao

---

George Dulikravich

---

Cheng-Xian Lin, Major Professor

Date of Defense: July 1, 2016

The thesis of John Goolcharan is approved

---

Interim Dean, Ranu Jung  
College of Engineering and Computing

---

Andrés G. Gil  
Vice President for Research and Economic Development  
and Dean of the University Graduate School

Florida International University, 2016

© Copyright 2016 by John Goolcharan

All rights reserved.

## DEDICATION

I dedicate this thesis to my parents, family and best friend. Without their patience, understanding, support, and most of all love, the completion of this work would not have been possible.

## ACKNOWLEDGMENTS

I would like to thank the members of my committee for their support, patience, and assistance in accomplishing all things pertaining to my thesis and masters experience. I would like to thank my major professor, Dr. Cheng-Xian (Charlie) Lin for his expert guidance and belief that I would complete my thesis, although at times the odds seemed to be stacked against us. I would also like to thank the other members of my committee, Dr. Dulikravich and Dr. Cao for lending their experience and expertise, to help guide me to prepare and defend my thesis. I would also like to thank the H2G fellowship provided through the Honors College at FIU for funding my pursuit of Masters of Science in Mechanical Engineering.

ABSTRACT OF THE THESIS

COMPUTATIONAL FLUID DYNAMIC ANALYSIS OF

MICROBUBBLE DRAG REDUCTION

by

John Goolcharan

Florida International University, 2016

Miami, Florida

Professor Cheng-Xian Lin, Major Professor

Microbubble drag reduction (MBDR) is an effective method to improve the efficiency of fluid systems. MBDR is a field that has been extensively studied in the past, and experimental values of up to 80% to 90% drag reduction have been obtained. The effectiveness and simplicity of MBDR makes it a viable method for real world applications, particularly in naval applications where it can reduce the drag between the surface of ships and the surrounding water. A two dimensional single phase model was created in ANSYS Fluent to effectively model the behavior of bubble laden flow over a flat plate. This model was used to analyze the effectiveness of MBDR based on the following factors: Reynolds number, types of gas injected, upstream flow velocity, upstream fluid type, density ratio, flow rate of injected gas, using air as the upstream injected fluid.

## TABLE OF CONTENTS

CHAPTER	PAGE
INTRODUCTION.....	1
BACKGROUND AND THEORY .....	3
LIMITATIONS OF EXISTING RESEARCH.....	16
SCOPE AND OBJECTIVES OF THESIS .....	16
METHODOLOGY.....	17
MODELLING.....	18
FLOW OVER FLAT PLATE AT MODERATE REYNOLDS NUMBER .....	20
SETUP OF GEOMETRY .....	20
SETUP OF MESH .....	20
DETERMINATION OF MESH SIZING AND MICROBUBBLE INJECTION ZONE .....	21
SETUP OF SIMULATION.....	23
MODELLING OF THE FLUID FLOW.....	23
MATERIALS SELECTION.....	24
CELL ZONE CONDITIONS .....	25
BOUNDARY CONDITIONS.....	25
ANALYSIS OF SIMULATIONS.....	25
DETERMINATION OF RE AND NON-DIMENSIONAL CONSTANTS ..	25
VALIDATION OF COMPUTED FRICTION COEFFICIENTS .....	27
MESH VALIDATION STUDY.....	28
EFFECT OF SURFACE ROUGHNESS.....	31
EFFECT OF AIR VS WATER AS THE FLUID IN THE FLOW .....	33
EFFECT OF DIFFERENT TURBULENCE INTENSITY .....	33
SCALED RESIDUALS.....	34
FLOW PROPERTIES.....	36
FLOW OVER FLAT PLATE AT HIGH REYNOLDS NUMBER.....	37

SETUP OF GEOMETRY .....	37
SETUP OF MESH, DETERMINATION OF SIZING AND MICROBUBBLE INJECTION ZONE.....	39
SETUP OF SIMULATION.....	42
MODELS.....	42
MATERIALS SELECTION.....	42
CELL ZONE CONDITIONS .....	43
BOUNDARY CONDITIONS.....	43
ANALYSIS OF SIMULATION .....	43
RESULTS .....	45
CONCLUSIONS.....	71
BIBLIOGRAPHY .....	74

## LIST OF TABLES

TABLE	PAGE
Table 1: The values determined and entered into ANSYS Mesh and used for the geometric progression calculations to determine the sizing of the new mesh .....	22
Table 2: The constants and input parameters used in the calculation of Re for the case with the Flow over a flat plate. ....	26
Table 3: Gas Properties for the Injected gases .....	31
Table 4: Density Ratio of the Upstream Fluids.....	33
Table 5: Turbulent kinetic energy, k, and the corresponding values of turbulent intensity, I. ....	34
Table 6: The values used for setting up the mesh sizing in ANSYS. This mesh was set up to analyze the case provided in the paper by Wendy et al. (2006).....	40

## LIST OF FIGURES

FIGURE	PAGE
Figure 1: Depiction of the boundary layer (Shapiro 2004).....	4
Figure 2: Boundary layer non-dimensional velocity profile (Shapiro, 2004).....	4
Figure 3: Moody diagram which relates pipe roughness, Re and friction factors (Moody, 1944) .....	11
Figure 4: The roughness function for sand-grain roughness for two models (Patel et al., 1991) .....	12
Figure 5: The effect of Density Ratio on the flow computational results from Lin et al. (2005).....	13
Figure 6: Wetted area ratios approximations used for aeronautical design calculations (Raymer, 1992) .....	15
Figure 7: Schematic of the geometry setup for the case with flow over flat plate according to Skudarnov and Lin (2006).....	20
Figure 8: Mesh Display for the case provided for the flow over flat plate with microbubble injected provided by Skudarnov and Lin (2006).....	21
Figure 9: Close up Display in ANSYS Mesh of the location of the first layer of cells over Wall 2 for the microbubble injection zone .....	23
Figure 10: The display from ANSYS Mesh showing the seamless integration of the manually created mesh over Wall 2 and the other zones .....	23
Figure 11: Course mesh 1 display for 80X48 .....	29
Figure 12: Course mesh 2 display for 100X56 .....	29
Figure 13: Fine mesh 1 display for 130X80 .....	30
Figure 14: Fine mesh 2 display for 150X96 .....	30
Figure 15: Figure showing scaled residuals for upstream velocity, $U_{\infty} = 4.2\text{m/s}$ .....	34

Figure 16: Figure showing scaled residuals for upstream velocity, $U_{\infty} = 10.9\text{m/s}$ .....	35
Figure 17: Display of Velocity over the surface for the Validation of the Model provided by Skudarnov and Lin (2006) .....	36
Figure 18: Schematic of the geometry setup for the case with flow over flat plate according to Wendy et al. (2006).....	37
Figure 19: The cross-sectional view of the flat plate in the test tunnel which shows the dimensions to be used Wendy et al. (2006).....	37
Figure 20: Enlarged view of the gas injection ports Wendy et al (2006).....	38
Figure 21: The display of the setup of the geometry in ANSYS .....	39
Figure 22: Extract from ANSYS showing the mesh used for the analysis for the extremely high Reynolds number case .....	41
Figure 23: Depiction of the first layer of cells to be used as the source term for the extremely high Reynolds number case .....	41
Figure 24: Enlarged View of the First layer of cells showing the seamless incorporation into the overall mesh for the extremely high Reynolds number case. ....	42
Figure 25: Computed Friction Coefficient - Comparison with Previous Results for Upstream Velocity $U=10.9\text{m/s}$ .....	45
Figure 26: Comparison of Computed Friction Coefficients for different mesh sizes at $U=10.9\text{m/s}$ .....	47
Figure 27: Comparison of Computed Friction Coefficients for different mesh sizes at $U=4.2\text{m/s}$ .....	48
Figure 28: Comparison of Different Gases acting as the source of microbubble injection for $U=10.9\text{m}$ .....	50
Figure 29: Comparison of Different Gases acting as the source of microbubble injection for $U=4.2\text{m/s}$ .....	51
Figure 30: Comparison of Roughness to Ratio of Drag Reduction for $U=10.9\text{m/s}$ .....	53

Figure 31: Comparison of Roughness to Ratio of Drag Reduction for $U=4.2\text{m/s}$ .....	54
Figure 32: Comparison of Air vs Water as the Fluid in the free stream with $\text{CO}_2$ microbubbles being injected for upstream velocity at $10.9\text{m/s}$ .....	57
Figure 33: Comparison of Air vs Water as the Fluid in the free stream with $\text{CO}_2$ microbubbles being injected for upstream velocity at $4.2\text{m/s}$ .....	58
Figure 34: Free stream turbulent intensity effect on drag reduction for $Q/UA=0.02$ . .....	60
Figure 35: Free stream turbulent intensity effect on drag reduction for $Q/UA=0.01$ .....	61
Figure 36: Comparison of Microbubble Drag Reduction as a Function of Distance for High Reynolds Number. This is a summary of the experimental Results .....	63
Figure 37: Comparison of Drag Reduction versus distance for High Reynolds Number at $U = 6 \text{ m/s}$ .....	65
Figure 38: Comparison of Drag Reduction versus distance for High Reynolds Number at $U = 12 \text{ m/s}$ .....	67
Figure 39: Comparison of Drag Reduction versus distance for High Reynolds Number at $U = 18 \text{ m/s}$ .....	69

## LIST OF SYMBOLS

SYMBOL	DESCRIPTION	UNIT
$\rho$	Density	$kg/m^3$
$\rho_m$	Mixture Density	$kg/m^3$
Re	Reynolds Number	Dimensionless
$\mu$	Viscosity	$Pa * s$
$\mu_m$	Mixture Viscosity	$Pa * s$
$Y_i$	Mass fraction	Dimensionless
Y	displacement height	m
K	Von Karman Constant	Dimensionless
$k^+$	Normalized Roughness mean height	m
k	Turbulent kinetic energy	$J/kg$
$\omega$	Specific dissipation rate	$1/s$
$C_f$	Skin Friction Coefficient	Dimensionless
$C_0$	Skin Friction Coefficient without microbubbles	Dimensionless
Q	Volume flow rate of microbubbles	$m^3/s$
$U_\infty$	Inlet fluid velocity	$m/s$
U	Fluid velocity	$m/s$
$\vec{U}$	Velocity Vector	$m/s$
$S_i$	Rate of species creation from sources	$kg/m^3 * s$
$\vec{J}_i$	Diffusion Flux	$kg/m^2 * s$
$Sc_t$	Schmidt number	Dimensionless
$\mu_t$	Turbulent Viscosity	$Pa * s$
L	Length of the plate	m
A	Area of the Plate	$m^2$

SYMBOL	DESCRIPTION	UNIT
$I$	Turbulence Intensity	Dimensionless
$\delta$	Boundary layer height	m
$F_D$	Drag Force	N
$S_{\text{wetted}}$	Wetted Area	$m^2$
$r$	Roughness coefficient	Dimensionless
$\tau_w$	Wall Shear Stress	$Pa$
$\Delta B$	Constant	Dimensionless
$u$	Dimensional velocity	$m/s$
$u^+$	Wall Function	Dimensionless
$u_\tau$	Shear Velocity	$m/s$
$y^+$	Wall Coordinate	Dimensionless

## ABBREVIATIONS AND ACRONYMS

ABBREVIATION	DESCRIPTION
CFD	Computational Fluid Dynamics
MBDR	Microbubble Drag Reduction
Re	Reynolds Number
RANS	Reynolds Average Navier Stokes
DR	Density Ratio
AFC	Active Flow Control
BL	Boundary Layer
AR	Aspect Ratio

## **INTRODUCTION**

In the real world, materials and systems interact with each other constantly. These interactions produce effects and results, which are determined by natural physical laws that govern the universe. Scientists, engineers and researchers spend time and money attempting to understand these laws and interactions in order to produce a desired effect. The interaction between fluids and solid objects is of particular interest. The fluid-solid interaction is present in everyday systems from the smaller motor vehicles to larger commercial items such as airplanes and ships.

Over time, the improvement of the efficiency of these transportation systems has been extensively studied by researchers. It is the desire for the efficiency of these systems to increase steadily so that economic and environmental gains can be made. It is evident that in fluid systems there is a resistance to fluid flow, which has been studied and labelled as drag, and has many different modes of affecting a system. In order to improve efficiency of a system this resistance, drag, needs to be decreased. As a result, drag reduction techniques from changing the shape of the system to the materials have been studied extensively. In this case, viscous or skin friction drag reduction through microbubble injection was studied.

To effectively utilize microbubble drag reduction (MBDR) as a valid method of drag reduction, its behavior must be completely understood to allow for it to be consistently predicted by designers. There currently exists several

experimental studies in MBDR. In most cases, the experimental results of a system can be effectively modelled analytically and predicted. Computational software was utilized to effectively determine and predict the behavior of the physical system. The challenge with modelling using software is that the models must be set up to closely mimic the conditions in reality. It is important that both the simulations and experimental results go hand-in-hand, which provides validation of the results obtained both by computational fluid dynamics (CFD) and experimental data.

This study aims at creating an effective computational model to be utilized in ANSYS Fluent software to effectively determine and predict the behavior of systems using MBDR. To model MBDR, Reynolds average Navier Stokes equations (RANS) were used. Additionally, the first layer of cells from the created mesh was treated as a gas source term, which approximates the behavior of injection of the microbubble gas. The species transport equation was used to determine the behavior of the particles in the flow. Finally, the viscous forces were prescribed using  $k-\omega$  turbulence modelling. The validity of the model was assessed by comparing it to previously obtained experimental and computational results for MBDR a range of Reynolds number cases. The model was subjected to an iterative process where it was set up then validated against the experimental results to determine if the results were significantly comparable. The simulations were run until the best setup was found, i.e. the statistical error was minimized, the model was deemed capable to be used for comparison against other cases.

## BACKGROUND AND THEORY

Drag can be considered as the net force in the direction opposite to that of fluid motion (Alexandrou, 2001). The boundary layer develops as the fluid flows over the surface. The boundary layer is understood to be a thin layer within the fluid adjacent to a wall or surface and develops due to viscous effects. The effect of the boundary layer can be seen in Figure 1 below. In this figure the velocity profile of the fluid as it approaches the flat plate is uniform, once it arrives at the solid surface the velocity profile changes instantly at the region closest to the wall. Within the boundary layer, the velocity profile of the fluid flow changes from zero at the solid wall or surface and gradually increases to a constant value, which is the velocity of the flow outside of this area. This effect is depicted in Figure 2, where the non-dimensional velocity  $U/U_e$  is almost zero at values close to the wall, i.e. for small values of  $y/\delta$ . As the fluid moves away from the wall and toward the top of the boundary layer, the velocity rapidly increases until it reaches the value of the velocity of the flow, i.e.  $U/U_e = y/\delta = 1$ . The zero velocity of fluid motion on the wall,  $y/\delta = 0$ , exists due to the non-slip condition of the solid wall which results in fluid particles becoming stuck to the wall. The boundary layer thickness,  $\delta$ , increases as the flow moves downstream.

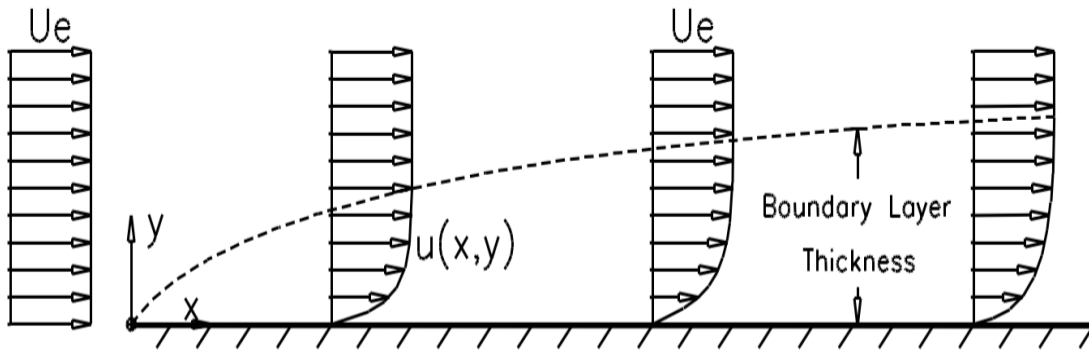


Figure 1: Depiction of the boundary layer (Shapiro 2004)

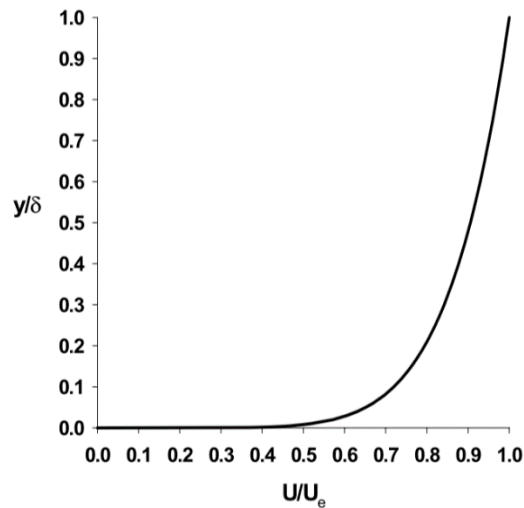


Figure 2: Boundary layer non-dimensional velocity profile (Shapiro, 2004)

There has been extensive research on the effect of microbubble gas injection as a method of drag reduction. The findings of the previous research have been staggering toward the positive, giving drag reduction values of up to 80 and 90 percentile values. The drag reduction mode occurs due to the microbubbles creating a lubricating film within the boundary layer which reduces the interaction between the fluid and the solid wall. Instead of the fluid particles sticking to the walls, they flow relative to the microbubbles. It is important to note

that this method of drag reduction, while theoretically effective can depend on several factors such as the flow rate, relative density, type of microbubble gas, etc.

The study by Skudarnov and Lin (2006) developed a single phase computational fluid dynamics model to observe the microbubble flow over a flat plate. In the Skudarnov and Lin (2006) study, the flow over the flat plate was taken to be water and microbubble injection being modelled as a mass source in the first layer of cells above the flat plate. By varying the properties of the gas used for the microbubble injection, the study sought to determine the role of mixture density and density ratio on the drag reduction. The skin friction coefficient can be defined as friction per unit area divided by head (Von Karman, 1934). This friction coefficient is dependent on the Reynolds number (Re).

To effectively determine the behavior of the flow, several systems of equations were utilized. Due to the turbulent nature of the model, Reynolds-averaged Navier-Stokes equations (RANS) (Skudarnov and Lin, 2006) were used to model the flow. RANS equations were used because they allow for the instantaneous flow properties to be obtained by looking at a combination of the average flow properties and the value of the perturbations.

$$\frac{\partial p}{\partial t} + \frac{\partial}{\partial x_i} (\rho_m u_i) = \dot{m} \quad (1)$$

$$\frac{\partial}{\partial t} (\rho_m u_i) + \frac{\partial}{\partial x_j} (\rho_m u_i u_j) = -\frac{\partial p}{\partial x_i} + \frac{\partial}{\partial x_j} \left[ \mu_m \left( \frac{\partial u_i}{\partial x_j} + \frac{\partial u_j}{\partial x_i} - \frac{2}{3} \delta_{ij} \frac{\partial u_l}{\partial x_l} \right) \right] + \frac{\partial}{\partial x_j} (-\rho_m \overline{u_i' u_j'}) + \dot{m} u_i \quad (2)$$

In the momentum conservation equation, the factor of  $-\frac{2}{3}$  shown was based on the Stokes hypothesis. The use of this equation by the solver can be a potential source of error in the computations. Stokes hypothesis claims that the bulk coefficient of viscosity is equal to zero which was taken as law for over a century and still remains a controversial topic in fluid mechanics (Dulikravich). While this factor can be approximated for monatomic gases, in reality, the factor is a much larger positive number. There is experimental evidence to show that this factor should be equal to almost 1000 for CO<sub>2</sub> (Truesdell, 1954). However, the term that is expressed here is related to the dilation factor, which is negligible when the expansion viscosity is very small (Sonin, 2001). In this case the model is observing flow which is not compressing on an extensive scale and the formulation recommended by the ANSYS solver and by Skurdanov and Lin (2006) can be taken as sufficient for this simple model.

In the equations shown, the density and viscosity are both of the mixture. This allows the calculations to incorporate the effects of both species. The mixture density was computed using the volume weighted mixing law. Based on the recommendation of the ANSYS theory guide, the mixture viscosity was computed using the mass fraction average of pure species viscosity since it was a component dependent model. This equation was also used by Skudarnov and Lin (2006) for computing the mixture viscosity and recommended in this model as well. The model sought to use simple methods which can effectively model the MBDR effectiveness and can be improved. There are other methods for mixture

viscosity that may yield better results, such as Kirchhoff's law for viscosity of mixtures.

$$\rho_m = \frac{1}{\sum_i \frac{Y_i}{\rho_i}} \quad (3)$$

$$\mu_m = \sum_i Y_i \mu_i \quad (4)$$

The two equation k- $\omega$  turbulence model provided by Wilcox was used.

These equations are useful as they allow for two additional equations to be used with the transport equations, do not require damping functions in the viscous sublayer and are not very stiff near the wall (Menter, 1992).

$$\frac{\partial}{\partial t} (\rho_m k) + \frac{\partial}{\partial t} (\rho_m k u_i) = \frac{\partial}{\partial x_j} \left( \Gamma_k \frac{\partial k}{\partial x_j} \right) + G_k - Y_k + S_k \quad (5)$$

$$\frac{\partial}{\partial t} (\rho_m \omega) + \frac{\partial}{\partial t} (\rho_m \omega u_i) = \frac{\partial}{\partial x_j} \left( \Gamma_\omega \frac{\partial \omega}{\partial x_j} \right) + G_\omega - Y_\omega + S_\omega \quad (6)$$

$$\mu_t = \rho k / \omega \quad (7)$$

$G_k$  represents the generation of turbulence kinetic energy due to mean velocity gradients.

$G_\omega$  represents the generation of  $\omega$

$\Gamma_k$  and  $\Gamma_\omega$  represents the effective diffusivity of k and  $\omega$  respectively

$Y_k$  and  $Y_\omega$  represent the dissipation of k and  $\omega$  respectively

$S_k$  and  $S_\omega$  are source terms

The boundary condition at the wall has the following values for k and  $\omega$ .

$$\frac{\partial k}{\partial n} = 0; \text{ where } n \text{ is the local coordinate normal to the wall} \quad (8)$$

$$\omega_w = \frac{\rho \mu_\tau}{\mu} \omega^+; \text{ where } \omega^+ = \min \left( 2500, \frac{6}{0.09 * (y^+)^2} \right) \quad (9)$$

The mixture density variation was due to the introduction of the gas species. The species transport equation allows for the effective modelling of the interaction between the gas species and the fluid flow. This equation allows both the convection and diffusion effects to be taken into account.

$$\frac{\partial}{\partial t}(\rho_m Y_i) + \nabla \cdot (\rho_m \vec{U} Y_i) = -\nabla \cdot \vec{J}_i + S_i \quad (10)$$

Where,  $S_i$  is the rate of creation of the  $i^{\text{th}}$  species

$\vec{J}_i$  is the diffusion flux of species  $i$ , given by the following relationship

$$\vec{J}_i = -\left(\rho_m D_{i,m} + \mu_t / S_{C_t}\right) \nabla Y_i \quad (11)$$

Where,  $S_{C_t}$  is the turbulent Schmidt number.

$\mu_t$  is the turbulent coefficient of viscosity.

$D_{i,m}$  is the diffusion coefficient for species  $i$  in the mixture.

It is well documented that Roughness affects the drag experienced by a fluid in motion. Generally, the roughness acts to restrict the fluid motion along the wall, causing the fluid particles to stick to the wall even further. This increases the viscous drag forces and the shear stresses, decreasing the value of the mean velocity profile in the boundary layer. In the solver, the law of the wall modified for roughness is used to analyze the behavior of the flow due to wall roughness (ANSYS). The law of the wall is modified to include an intercept  $\Delta B$ , which is dependent on the roughness height,  $k^+$ , and the roughness constant,  $r$ . This treatment of the law use the flow regime definitions proposed by Nikuradse (1933) and White (1974), where  $k$  is the mean roughness height and  $+$  indicates the normalization of the roughness height with the wall unit (Deutsch et al., 2004). The relationship is seen using the system of equations.

$$u^+ = \frac{1}{K} \ln y^+ - \Delta B \quad (12)$$

The wall coordinate is defined by

$$y^+ = \rho y u_\tau / \mu \quad (13)$$

The wall function is defined by

$$u^+ = u / u_\tau \quad (14)$$

The friction velocity is given by

$$u_\tau = \sqrt{\tau_w/\rho} \quad (15)$$

The intercept is defined using the relationship below.

$$\Delta B = \frac{1}{K} \ln f_r \quad (16)$$

In this case  $f_r$  is a roughness function which is dependent on the roughness conditions as there is currently no universal function for all cases.

There is good agreement for  $\Delta B$  and the values of  $k^+$ . Using the relationships by Nikuradse (1933) the following relationships are obtained.

$$\begin{aligned} 0 < k^+ < 2.25 & \quad - \textit{dynamically smooth} \\ \Delta B & = 0 \end{aligned} \quad (17)$$

$$\begin{aligned} 2.25 < k^+ < 90 & \quad - \textit{transitionally rough} \\ \Delta B & = \frac{1}{K} \ln \left[ \frac{k^{+2.25}}{87.75} + rk^+ \right] \times \sin[0.4258(\ln k^+ - 0.811)] \end{aligned} \quad (18)$$

$$\begin{aligned} 90 < k^+ & \quad - \textit{fully rough} \\ \Delta B & = \frac{1}{K} \ln(1 + rk^+) \end{aligned} \quad (19)$$

The work performed by Kunz, Deutsch and Lindau (2003) adapted an unstructured three dimensional multiphase phase flow CFD model for high Reynolds number external flows with microbubble drag reduction. The finding of this paper confirmed that the use of MBDR was an effective method for drag reduction. The study showed that the turbulent kinetic energy is decreased through microbubble breakup in the liquid phase reducing skin friction (Kunz et al., 2003). This model was used to analyze quasi one dimensional flows, two

dimensional flows over a flat plate and a three dimensional analysis of high lift hydrofoil (Kunz et al., 2003). The 2D model analyzed was similar to the model in the numerical analysis performed by Skudarnov and Lin (2006).

The models created by Skudarnov and Lin (2006) and Kunz et al. (2003) followed the experiments performed by Merkle and Deutsch (1992).

Researchers set up several experiments to observe the factors that affect microbubble drag reduction and found that these factors were: bubble size, trajectory of the bubble cloud and volumetric flow rate of the flow.

Further research was performed by Sayyaadi and Nematollahi (2013) concerning the optimum gas injection rates. A 70cm catamaran model was used to model the flow around a ship and it was determined that suitable injection rates reduce drag by approximately 5-8%. It was interesting to note that excessive air injection rates decrease the drag reduction effect.

The use of computational fluid dynamics (CFD) to determine the effects of fluid flow are not perfect and limitations exist both in the numerical algorithm and those inherent in the physical model according to Patel (1998). The limitations of the modelling are applied to several cases and of particular interest are the limitations related to surface roughness. In most cases the surface roughness is identified by using figures such as the Moody diagram seen in Figure 3, which relate the Reynolds number ( $Re$ ), roughness and friction factors. These diagrams allow for the surface roughness to be taken into account which is then applied to the flow transport equations. The modelling used to analyze the flow

needs to take the roughness into account to accurately determine the behavior of the system. The k- $\omega$  turbulence model took into consideration the data obtained from equation (8) to determine the wall function. There are other means of taking the effect of roughness into consideration, which gave similar results shown in Figure 4, which compared several roughness models (Patel, 1991). The results obtained by CFD, particularly as it relates to imperfect conditions such as roughness, need to be verified with real life conditions, because in CFD there is a certain uniformity that is assumed with imperfections. However, CFD analysis gives a fairly accurate prediction of the behavior of the flow.

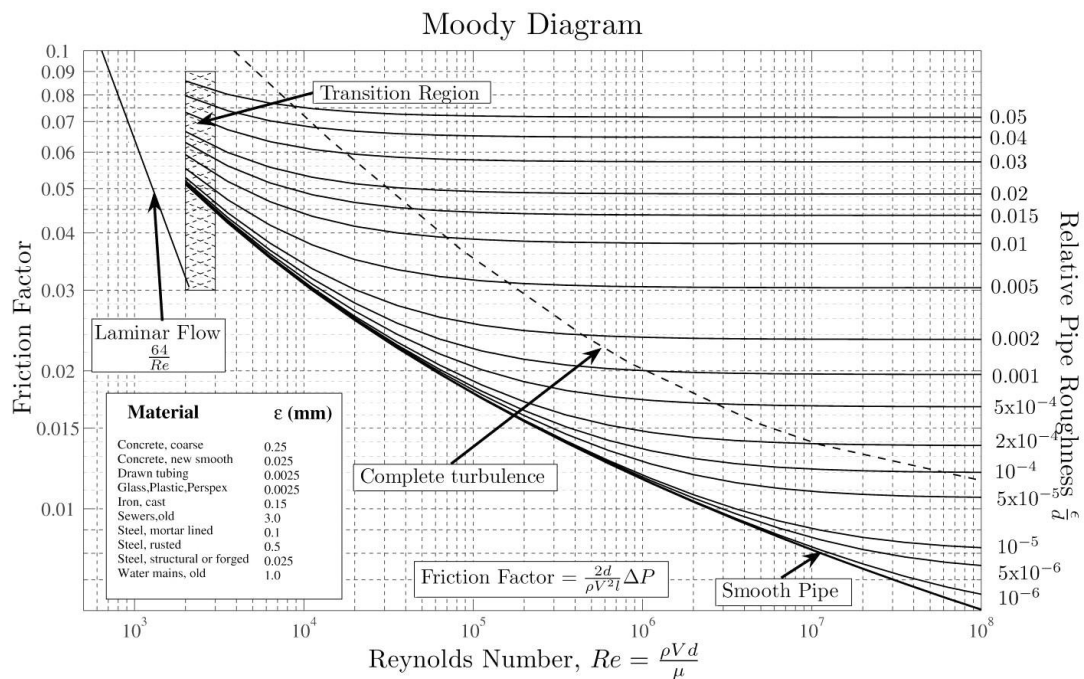


Figure 3: Moody diagram which relates pipe roughness,  $Re$  and friction factors (Moody, 1944)

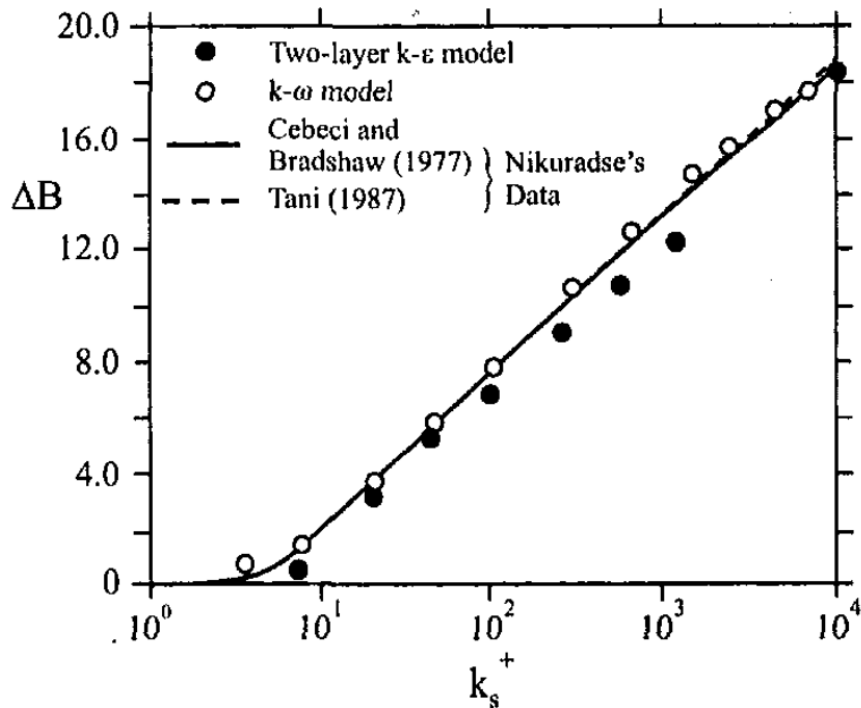


Figure 4: The roughness function for sand-grain roughness for two models (Patel et al., 1991)

As it relates to the MBDR effect of the flow, the density ratio, DR, affects the effectiveness of the performance. The density ratio as shown in equation (20) is the ratio between the density of the fluid that flows parallel to the plate,  $\rho_{\text{fluid}}$ , to the density of the injected gas,  $\rho_{\text{gas}}$ . Deutsch et al. (1992) experimentally observed the effect of DR by injecting various gases onto an axisymmetric body subjected to a wide range of water flow velocities,  $U_\infty$ , and tunnel pressures. This study found that for the gases with lower densities the drag reduction capabilities were improved, although the differences in drag reduction capabilities were small. This effect was also studied by Lin et al. (2005), by simulating flow over a flat plate. This study found that for low gas injection rates the effect of density ratio was negligible on MBDR. For high gas injection rates, improved

drag reduction capabilities with increasing density ratio was found. This indicated that simple mixture density variation effect is a major factor in MBDR. The results are seen in Figure 5 which clearly shows the effect of changing the DR.

$$\text{Density Ratio, } DR = \frac{\rho_{\text{water}}}{\rho_{\text{gas}}} \quad (20)$$

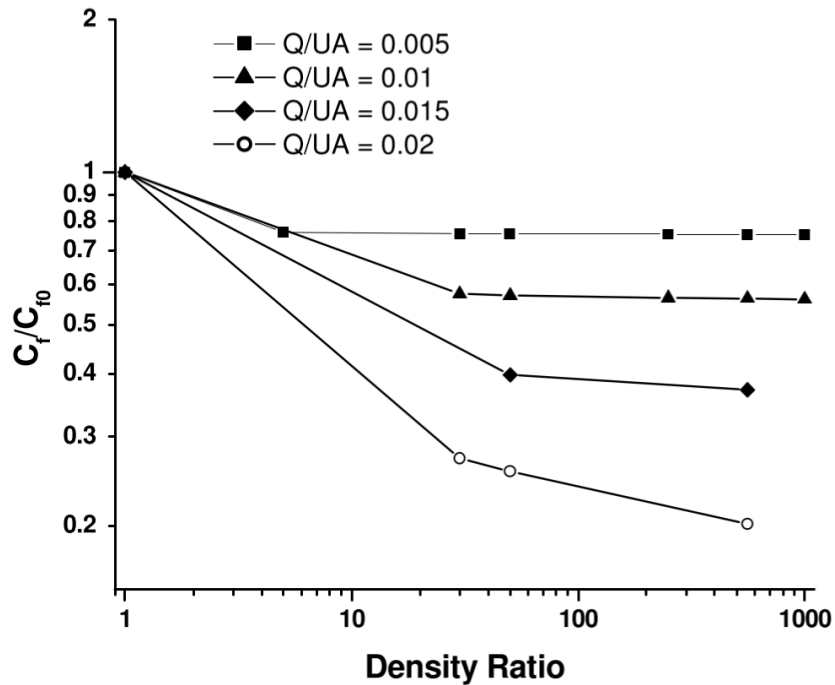


Figure 5: The effect of Density Ratio on the flow computational results from Lin et al. (2005)

Skudarnov and Lin (2005) investigated the effect of the free stream turbulent intensity on MBDR effectiveness. That paper used the case of flow over a flat plate and determined the behavior of MBDR for two cases for values of  $Q/UA$ . That paper compared the effect of the turbulent intensity,  $I$ , across a range of density ratios, DR. The turbulent intensity is derived from the equation below, which computes the value of  $I$  as a function of turbulent kinetic energy,  $k$ ,

and upstream velocity,  $U$ . The turbulent kinetic energy was found to have a significant effect on the drag reduction. It was found that the turbulent intensity at the inlet was inversely proportional to the MBDR effectiveness Skudarnov and Lin (2005).

$$I = \frac{\sqrt{2/3k}}{U} \quad (21)$$

There are several other methods for reducing drag in fluid flows. The equation below gives a model for determining the drag. The equation gives the relationship between the coefficient of drag,  $C_D$ , to the drag force,  $F_D$ , fluid density,  $\rho$ , fluid velocity,  $U$  and the characteristic length of the body,  $L$  (Tritton, 1998). In the case of MBDR, the introduction of a secondary fluid, i.e. the microbubbles, cause the value of the density to be manipulated. This changes the value of the drag seen in the equation below. Likewise, varying the other factors in the equation, it is possible that drag reduction can be achieved. One such method is by manipulating the characteristic length,  $L$ . This manipulation is achieved by changing the size and shape of the body that is subjected to the fluid flow. This is a method that is employed extensively, particularly in the automotive and airline industries to increase efficiency (Pandian, 2013).

$$F_D = 1/2 \rho U^2 L^2 C_D \quad (22)$$

In addition to altering the actual size of the object that is in the fluid flow, the drag can be reduced by reducing the wetted area,  $S_{\text{wetted}}$ . This can be seen via the equation below, which is similar to the one previously but is used for the

skin friction drag and replaces  $L^2$  with  $S_{wetted}$ . The wetted area,  $S_{wetted}$ , is the area of the body that is exposed to the fluid flow (Raymer, 1992). This is a concept that is used in calculations for designs of automotive, aeronautical and piping systems. Particularly in the case of aeronautical design, the wetted area is approximated using historical information and ratios (Raymer, 1992). Using the information presented here it is possible to design systems that would have minimum drag forces through the reduction of the wetted area. Active Flow Control (AFC) for wetted area reduction is used to reduce drag through reduction of the wetted area (Washburn, 2010).

$$F_D = \frac{1}{2} \rho U^2 S_{wetted} C_D \quad (23)$$

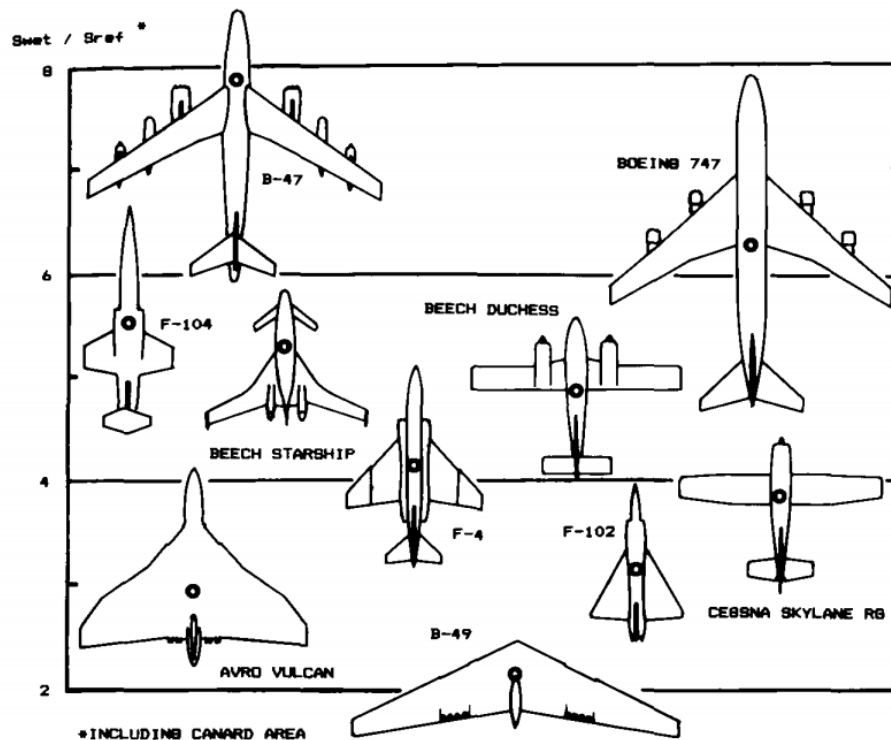


Figure 6: Wetted area ratios approximations used for aeronautical design calculations (Raymer, 1992)

## **LIMITATIONS OF EXISTING RESEARCH**

The existing work, while effective up to this point has limitations. In the previously performed experiments, a limitation is that only a limited number of geometries were tested and a limited number of combinations of fluids were tested. It would be useful for experiments to be performed to determine the MBDR effectiveness for different surfaces, such as an airfoil. A limit of the previous work that was performed was that MBDR used mainly liquid-gas interactions. Once MBDR can be validated for other interactions, particular gas-gas systems, new avenues for MBDR utilization can be opened, including applications in the aerospace industry.

There are limitations when using CFD analysis, which are built into the models (Patel, 1998). These limitations exist in the range of  $Re$  that a model can produce valid results and the physical constraints of the model (Patel, 1998). Physical limitations exist in the difficulty to model certain conditions which may exist in reality, for example roughness. Additionally, there can be computational error. Modelling makes use of equations which can give a mathematical understanding of the real world conditions. In reality, however, when performing calculations errors exist which may propagate throughout the model, causing the results to deviate from the expected results.

## **SCOPE AND OBJECTIVES OF THESIS**

The aim of this thesis was to analyze the previously studied works in MBDR. The results were compared to results obtained by CFD modelling and

analysis of the conditions using ANSYS Fluent. The key comparisons were performed based on the works by Skudarnov and Lin (2006), Skudarnov and Lin (2005), Wendy et al. (2006), Deutsch and Fontaine (1992), Kunz et al. (2003). In these previous works, the effectiveness of MBDR was observed by manipulating factors of Reynolds number, types of gas injected, upstream flow velocity, density ratio, and flow rate of injected gas. This thesis aims at validating that MBDR can be model effectively using a two dimensional single phase CFD model in ANSYS. The validation was performed by comparing the previous results to the results obtained from the MBDR model. The validation of this model allowed for prediction and analysis of systems with MBDR. The thesis aimed at validating the previous experimental data for MBDR using the model by varying several factors that affect the MBDR performance. Additionally, observing MBDR for varying upstream fluid type which was a factor that had not been previously studied. These factors were compared using flow over a flat plate and comparing for comparatively low and high Reynolds number cases. The study aimed at determining the validity and limitation of using a two dimensional single phase CFD model for analyzing MBDR.

## **METHODOLOGY**

Computational Fluid Dynamics (CFD) is a field which, while effective, can have many pitfalls which can easily be a stumbling block to the investigator. It is very important that the correct software and modelling be used. To perform CFD analysis, there are several commercially available software and code can be

written by the researcher. For the study, ANSYS Fluent program was used to model and simulate the system behavior for the purpose of simply comparing and testing the theory, and perform analysis. This software was chosen due to its strong track record, commercial availability and due to the fact that it was used to model the system by Skudarnov and Lin (2006).

## **MODELLING**

As previously stated, ANSYS software was used to develop the systems for simulations and analysis. The model used was a two dimensional single phase computational model Skudarnov and Lin (2006). To effectively determine the behavior of the system, modelling was setup in a two dimensional coordinate system with the geometry set so that it appears that the system is being observed in a cross-sectional manner. In the works performed by Skudarnov and Lin (2006) and Kunz et al. (2003), a similar interpretation was used to model flow over a flat plate for the purpose of studying MBDR. Using this approach allows for a simplified set up which can still allow for accurate simulation of the effect of MBDR.

The turbulence model was selected to be the  $k$  and  $\omega$  model. This is advantageous as it allows for two additional equations to be used together with the transportation equations which will account for the turbulent effects of the flow such as convection and diffusion of turbulent energy. Additionally, the model does not require damping functions in the viscous sublayer and the equations are not very stiff near the wall (Menter ,1992). In the model,  $k$ ,

accounts for the turbulent kinetic energy and  $\omega$ , is the specific dissipation rate which determines scale of the turbulence.

The species transportation equations were used to model the behavior of the particles in the fluid flow. This interpretation was useful when understanding the interaction between the fluid and the gas. The species transportation is used for constant density incompressible flow. This equation solves for convection, diffusion and source terms to model across the mesh how the microbubbles are carried in the fluid flow.

## FLOW OVER FLAT PLATE AT MODERATE REYNOLDS NUMBER SETUP OF GEOMETRY

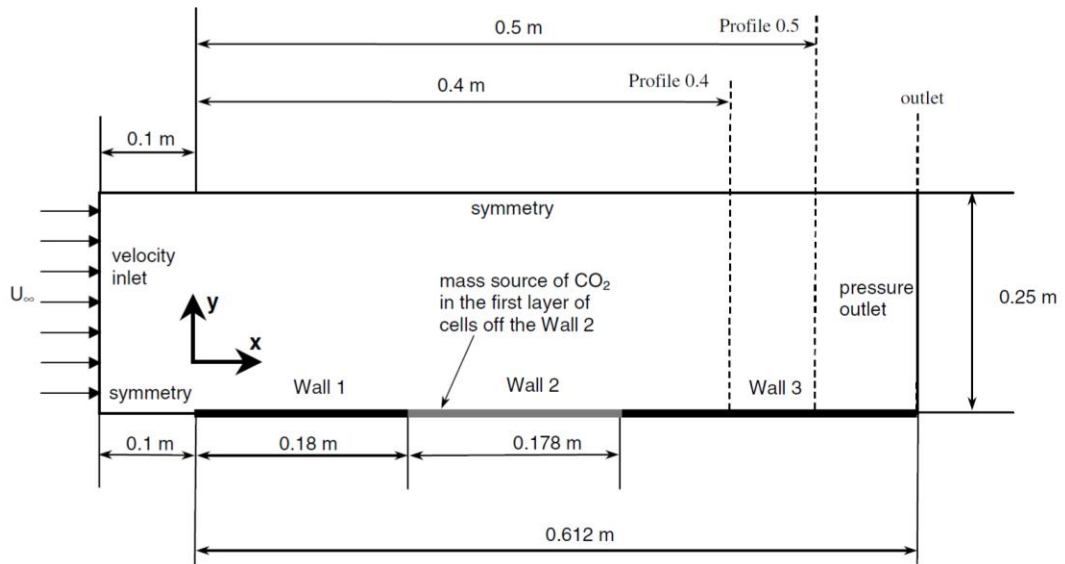


Figure 7: Schematic of the geometry setup for the case with flow over flat plate according to Skudarnov and Lin (2006).

For the flow over a flat plate at moderate  $Re$ , the setup of the geometry was identical to the geometry used by Skudarnov and Lin (2006). The system was set up in such a manner that it appears to be observed through a cross-sectional cut. The dimensions and configuration of the geometry was shown in Figure 7.

## SETUP OF MESH

The mesh was setup to mimic the 113X65 mesh that was used in the paper provided by Skudarnov and Lin (2006). This mesh was created so that there would be a large concentration of mesh elements close to the plate area in the horizontal direction and at transition zones in the vertical directions which

were taken as the areas at the wall transitions. This information can be seen in Figure 8 below which is taken from the ANSYS display.

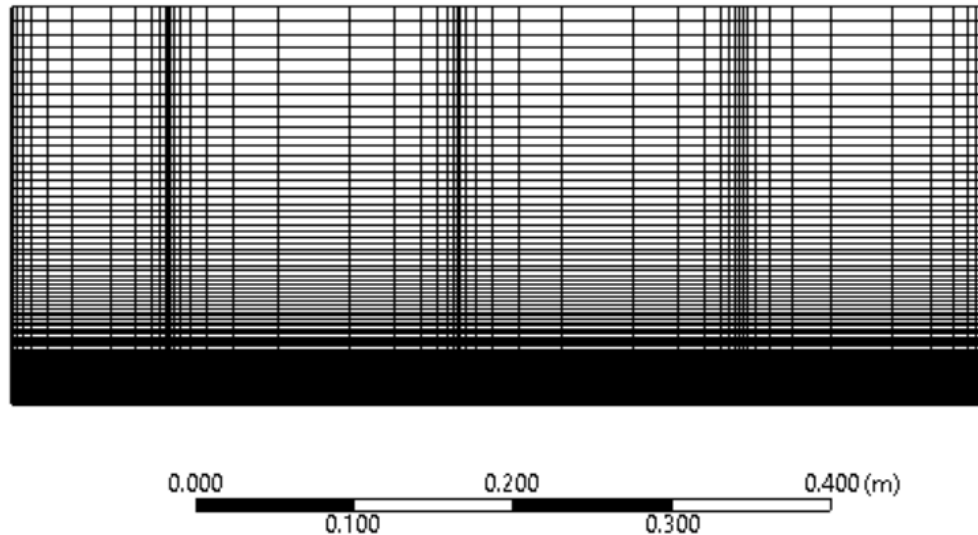


*Figure 8: Mesh Display for the case provided for the flow over flat plate with microbubble injected provided by Skudarnov and Lin (2006).*

### **DETERMINATION OF MESH SIZING AND MICROBUBBLE INJECTION ZONE**

To properly simulate the microbubble gas injection over Wall 2, the first layer of cells of the mesh over Wall 2 was set as a separate zone and had to be sized manually. An important factor in selecting the mesh factors was determining a mesh size which would be small enough to capture changes in the flow and the boundary layer. Treating the mesh over Wall 2 a separate cell zone allows for that zone to be taken as the source term. Proper sizing of this mesh allows for seamless integration between the mesh over Wall 2 and the other area. To perform this action factors such as: the number of cells,  $n$ , bias factor,  $b$ , overall height,  $S_n$ , and bias type were predetermined and had to be treated as constants in a geometric progression. Performing the calculations shown below

gives the height of the first layer of cells,  $a_{113}$ , as well as the new bias factor for the remaining cells in the direction of the y-axis,  $b_{112}$ .

Description	Symbol	Value	Unit
Overall height	$S_n$	0.25	m
Bias Factor	$b$	50	Dimensionless
Number of Cells	$n$	113	Dimensionless

Table 1: The values determined and entered into ANSYS Mesh and used for the geometric progression calculations to determine the sizing of the new mesh

$$b = a/a_n = a/ar^n = 1/r^n = 50 \quad (24)$$

$$r = \sqrt[n]{1/50} = \sqrt[113]{1/50} = 0.966 \quad (25)$$

$$S_n = \frac{a(1-r^n)}{(1-r)} \quad (26)$$

The application of the above equations and rearrangement to find the factor for determining the progression of the sizing,  $a$ , the height of the first cell,  $a_{113}$ , and the new value of the bias factor for the 112 remaining cells over Wall 2,  $b_{112}$ .

$$a = \frac{S_n(1-r)}{(1-r^n)} = 0.00867 \quad (27)$$

$$a_n = ar^n \quad (28)$$

$$a_{113} = 0.0001734m$$

$$b_{112} = a/a_n = a/ar^n = 1/r^n = 1/(0.966)^{112} = 48.2986366 \quad (29)$$

The manual creation of this mesh using the mathematical principles allowed for the different zone meshing to become integrated to each other seamlessly. The figures below show the seamless mesh integration between the zones; Figure 9 shows the location of the first cell in the mesh over wall 2 and

Figure 10 shows a close up view of the overall mesh shown in Figure 8 at the location of the transition between wall 1 and wall 2.

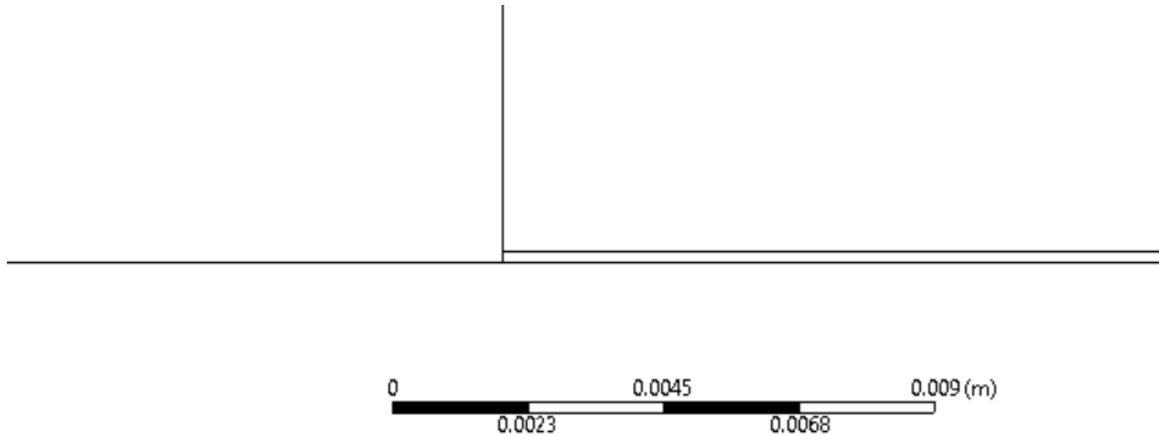


*Figure 9: Close up Display in ANSYS Mesh of the location of the first layer of cells over Wall 2 for the microbubble injection zone*

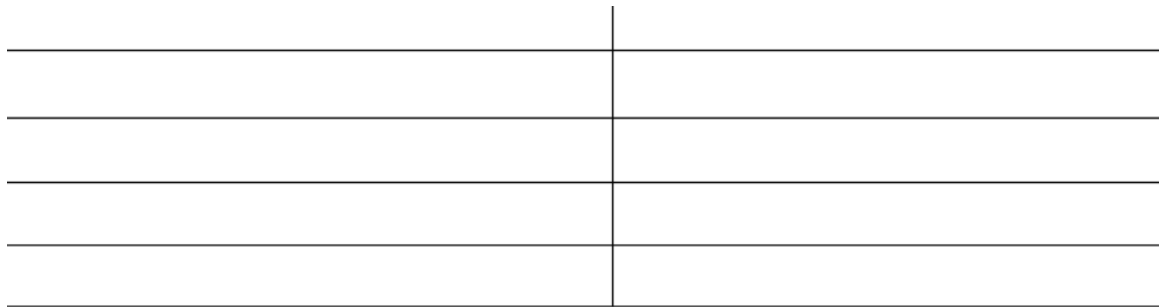


*Figure 10: The display from ANSYS Mesh showing the seamless integration of the manually created mesh over Wall 2 and the other zones*

## **SETUP OF SIMULATION MODELLING OF THE FLUID FLOW**

Once the geometry setup was completed, the system was set up using ANSYS Fluent. At this point the equations to be used in the computational model were selected. For this case, the following models were selected and based on the values reported in the work by Skudarnov and Lin (2006):

1. Viscous – k and  $\omega$
2. Species Transportation

As previously stated, using the k and  $\omega$  model for the turbulence modelling allows for two additional equations to be used together with the transportation equations which will account for the turbulent effects of the flow such as convection and diffusion of turbulent energy. The values of k and  $\omega$  were chosen as  $1.2 \times 10^{-5}$  and  $1.2 \times 10^{-3}$  respectively and these values were chosen for the initialization of the system.

The Species Transportation in the modelling of the system was utilized to allow for the behavior of the gas to be correctly modelled. In the species transportation model, each fluid's local mass fraction is predicted using a convection-diffusion equation for the species.

## **MATERIALS SELECTION**

It was important that the materials be selected correctly to model the system. The material properties such as mass, density, and viscosity were important as they would be used in the computational model. The materials selected were water (liquid) and carbon dioxide for the mixture model which allowed for the model to accurately predict the behavior of the two fluids interacting as a mixture. For the fluid zones, water was chosen as the upstream fluid and carbon dioxide gas to act as the injected microbubbles.

## **CELL ZONE CONDITIONS**

The cell zones were set up to accurately mimic the flow conditions and microbubble injection. There were two distinctions for the cell zones with both zones set as fluid. First zone assignment was the microbubble injected area, which was assigned to be a source term for CO<sub>2</sub> which was set to be at a rate which matched the values by Skudarnov and Lin (2006). The second cell zone to be assigned, was the area compliment to that area set as the microbubble injection zone, this area was set as a fluid zone.

## **BOUNDARY CONDITIONS**

The inlet was set as a velocity inlet boundary condition which used values of 10.9  $m/s$  and 4.2  $m/s$  which were consistent to the values used by Skudarnov and Lin (2006) and Kunz et al. (2003). Symmetry boundary conditions were used at the leading edge of the domain as well as the far field of the system which effectively predicts the behavior of the flat plate in a water channel. The no-slip boundary condition is applied to all walls which makes the plate to act as a flat plate. The constant pressure boundary condition is applied at the outlet. The initialization of the system used the inlet as the reference point which allowed the simulation to adopt the values of  $k$  and  $\omega$  as the initial guess.

## **ANALYSIS OF SIMULATIONS**

### **DETERMINATION OF RE AND NON-DIMENSIONAL CONSTANTS**

The Reynolds number,  $Re$ , is an important factor as it represents the non-dimensional ratio of the inertial forces to the viscous forces of a flow. Due to  $Re$

being a non-dimensional constant, allows for general principles to be assessed for different systems.  $Re$  was determined using the dimension and layout shown in Figure 7.

$$\text{Reynolds Number, } Re = \frac{\rho U_{\infty} L}{\mu} \quad (30)$$

This equation uses the parameters shown in Table 2 which used the fluid properties of the water which was the fluid over the flat plate for the values of density  $\rho$  and viscosity  $\mu$ . The characteristic length,  $L$ , was designated as the length of the plate, this designation was consistent with previous research for the determination of  $Re$ . The upstream velocity had two designations which were  $U_{\infty} = 10.9 \text{ m/s}$  and  $4.2 \text{ m/s}$ . Using these values in the calculations the two unique numbers for the value of  $Re$  can be seen in Table 2.

Table 2: The constants and input parameters used in the calculation of  $Re$  for the case with the Flow over a flat plate.

Property	Value	Unit
Density, $\rho$	998	$kg/m^3$
Length, $L$	0.612	$m$
$U_{\infty,10.9}$	10.9	$m/s$
$U_{\infty,4.2}$	4.2	$m/s$
Viscosity, $\mu$	$1.003 \times 10^{-3}$	$kg/m \cdot s$
$Re_{10.9}$	$6.64 \times 10^6$	Dimensionless
$Re_{4.2}$	$2.56 \times 10^6$	Dimensionless

For the comparison of the data shown in the resulting figures, the values for friction coefficient and the flow were assigned non-dimensional values. Along the y-axis, the non-dimensional coefficients for the ratio of the friction coefficients

over Wall 3 was determined by dividing the friction coefficient over the wall for the case of zero microbubble injection,  $C_0$  by the friction coefficient over Wall 3,  $C_f$ . Along the x-axis the flow was represented by the non-dimensional ratio  $Q/UA$ . This ratio relates the volumetric flow rate of the injected gas,  $Q$ , to the velocity of water,  $U$ , over the specified area,  $A$ .

## VALIDATION OF COMPUTED FRICTION COEFFICIENTS

A major determination in the validity of the model was the ability to give results similar to that of the previously studied experimental and simulated values. Figure 25 and **Error! Reference source not found.** shows the previously obtained experimental results by Merkle and Deutsch (1992). On the same figure the computational results provided by Skudarnov and Lin (2006) and Kunz et al. (2003) were compared. The simulation was run for two cases of the upstream velocity,  $U_\infty = 10.9 \text{ m/s}$  and  $4.2 \text{ m/s}$ . For both cases the results obtained matched closely to the values obtained both experimentally and the previous results showing good agreement for the model in terms of being able to accurately predict the behavior of the system.

In Figure 25 to **Error! Reference source not found.** the relatively close results were displayed, especially at areas of high and low values of  $Q/UA$ . The average error between the values obtained by Skudarnov and Lin (2006) and the present results in these regions are very small and can be considered to be negligible. However, as the values of  $Q/UA$  increased the error increased.

## **MESH VALIDATION STUDY**

To confirm the results, a mesh validation study was conducted. The 113X65 mesh that was used in the paper provided by Skurdanov and Lin (2006) was taken as the baseline for comparison. This mesh was created so that there would be a large concentration of mesh elements close to the plate area in the horizontal direction and at transition zones in the vertical directions which were taken as the areas at the wall transitions and the first layer of cells over Wall 2 as the source of the microbubbles injected. Using this similar structure 4 other simulations were run using varying mesh sizes. Two courser mesh sizes were chosen and designated as Course Mesh 1 - 80X48 and Course Mesh 2 - 100X56 which can be seen in Figure 11 and Figure 12 respectively. Additionally, two finer mesh sizes were chosen as Fine Mesh 1 – 130X80 and Fine Mesh 2 – 150X96 shown in Figure 13 and Figure 14 respectively. These mesh sizes were also manually setup for the source term over Wall 2 in a similar manner as the 113X65 mesh.

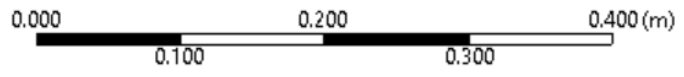
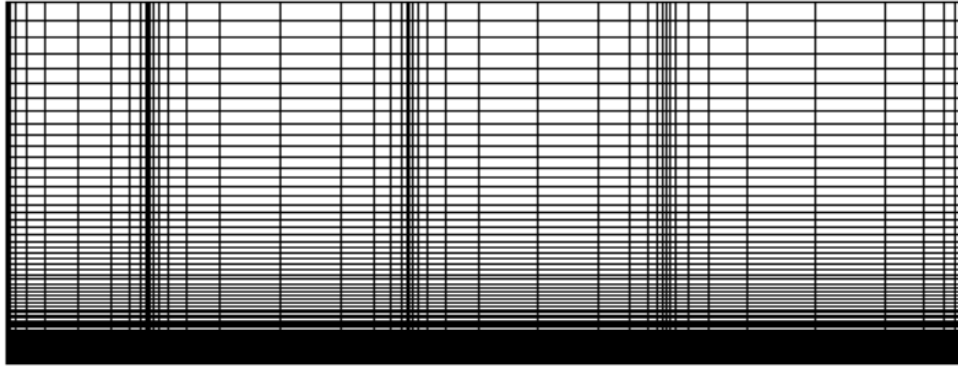


Figure 11: Course mesh 1 display for 80X48

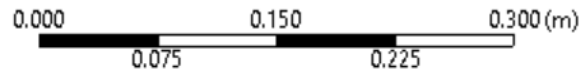
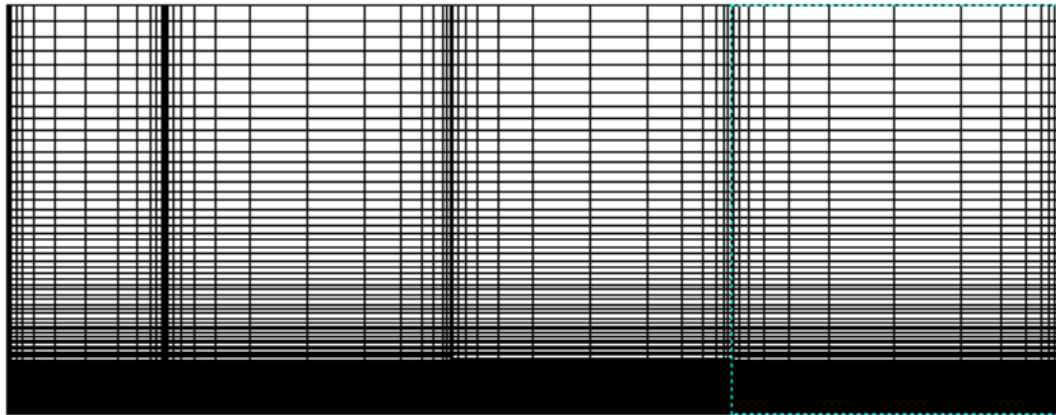


Figure 12: Course mesh 2 display for 100X56

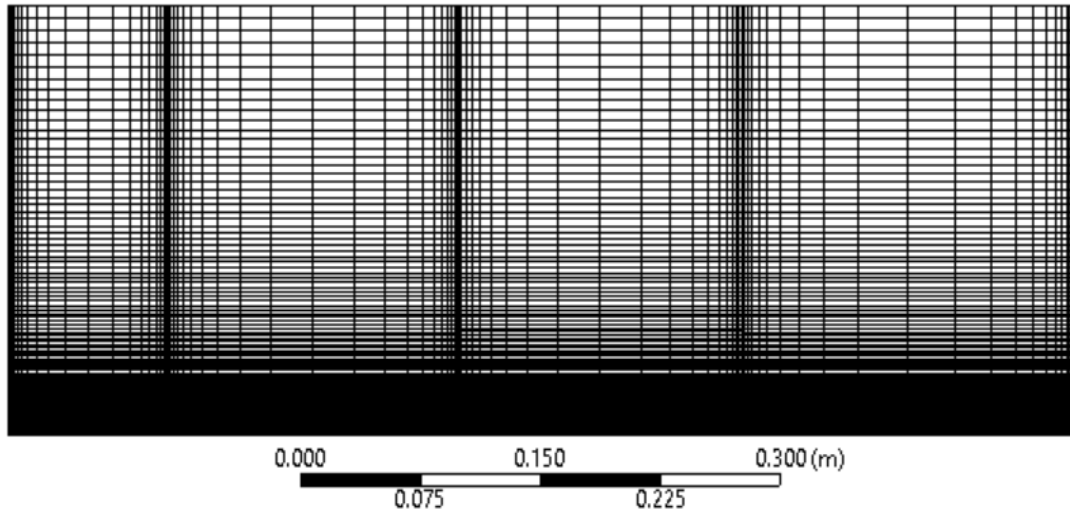


Figure 13: Fine mesh 1 display for 130X80

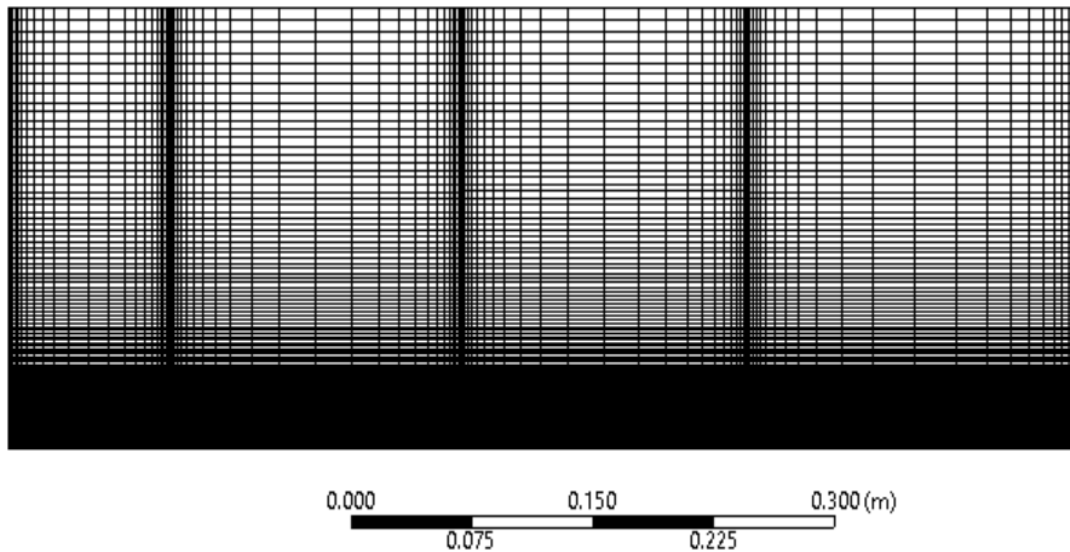


Figure 14: Fine mesh 2 display for 150X96

## EFFECT OF DIFFERENT INJECTED GASES

It is clear from the previous research done by Deutsch et al (1992) that the type of gases that is used to produce the microbubble drag reducing effect affects the MBDR effectiveness. Using the system setup as Skudarnov and Lin (2006) the effect of the injected gas was determined. The same gases that were

used in the experimental setup by Deutsch et al (1992) were used for the comparison, with the exception of sulphur-hexafluoride, due to the limitations of the ANSYS software, as its material properties were not available. The material properties of each of the gases are displayed in Table 3.

*Table 3: Gas Properties for the Injected gases*

<b>Gas</b>	<b>Density (kg/m<sup>3</sup>)</b>	<b>Density Ratio</b>
Helium	0.165	6048.485
Air	1.2	831.6667
Argon	1.65	604.8485
Carbon Dioxide	1.83	545.3552

The results of this system is displayed in Figure 28 and Figure 29 which captured the two values of  $U_{\infty}$ . There was strong correlation between the expected effects of the change in gases which is dependent on the density ratio. In the previously studied experimental results produced by Deutsch et al (1992) and in the simulated results there was strong agreement on two factors. Firstly, the drag reduction effect is improved for higher density ratio. This means that the lower the density of the injected gas, the better the performance, which is why He was the best performer of the system. This effect is in agreement with other experimental and in particular the simulated results produced by Skudarnov and Lin (2006). Secondly, the effect of change of gases were very small.

## **EFFECT OF SURFACE ROUGHNESS**

It is clear that the roughness of the wall will affect the behavior of the system. According to Deutsch et al (2004), the percentage of drag reduction was

increased for the roughness coefficients. It is important to note that the actual skin friction coefficients can be higher for higher values of roughness, while simultaneously the percentage of drag reduction was greater. The roughness height, which is the average height of the impurities on the surface, was kept constant for all the trials as 0.0001734m (173 $\mu$ m) which represents the first layer of cells for the system. The roughness coefficients, which is the non-dimensional representation of the effect of the non-uniformity of the surface were changed for values ranging from 0 to 1.

The default mesh of 113X65 was used for this case and the fluid for the injection of the microbubbles was carbon dioxide. The reason why the roughness adds to the effect of the microbubble drag reduction is because it helps the microbubbles stay on the surface of the plate aiding to the “lubricating effect” of the microbubbles. The results were given in Figure 30 and Figure 31. Additionally, roughness of the wall fits into the transportation equations affects the change in pressure, which can be determined from experimental results from graphics such as the Moody diagram.

The almost perfect results negated the concerns of Patel (1998) as it took into consideration the wall conditions shown by equation (8). This wall function may still not be enough for the system to be considered perfect as there are several other factors due to surface roughness which are not taken into consideration. One such is the uniformity of the surface roughness and the resulting separation and recirculation of the flow in certain areas along the

surface of the plate. This model is sufficient enough to give preliminary results to predict the behavior of the flow.

### **EFFECT OF AIR VS WATER AS THE FLUID IN THE FLOW**

The effect of air vs water was computed using the 113X65 mesh sizing. The results obtained and displayed in Figure 32 and Figure 33, which capture both values of  $U_\infty$ . The obtained results were consistent with what is expected from the experimental results, and previously obtained results which show a dependence on the density ratio. In the simulated cases, the density ratio ( $DR = \rho_{CO_2} / \rho_{fluid}$ ) affects the drag reduction capabilities. It is widely proved that the drag reducing capabilities are increased for lower density ratios. Comparing the density ratios we get the values shown in Table 4 for the gases used.

*Table 4: Density Ratio of the Upstream Fluids*

<b>Gas</b>	<b>Density (kg/m<sup>3</sup>)</b>	<b>Density Ratio</b>
Air	1.2	1.525
Water	1000	0.00183
Carbon Dioxide	1.83	

### **EFFECT OF DIFFERENT TURBULENCE INTENSITY**

The effect of the turbulent intensity was validated in comparison to the previous results from Skudarnov and Lin (2005). The turbulent kinetic energy,  $k$ , values were manipulated to give different values of turbulent intensity,  $I$  for constant  $U = 10.9 \text{ m/s}$  shown via the equation below. A summary of this can be seen in the table below.

$$k = \frac{3}{2} (UI)^2 \quad (31)$$

Table 5: Turbulent kinetic energy,  $k$ , and the corresponding values of turbulent intensity,  $I$ .

$k$	$I$ (%)
1.00E-03	0.24
1.00E-02	0.75
5.00E-02	1.67
1.00E-01	2.37
1.00E+00	7.49

The results displayed in Figure 34 and Figure 35 which give two unique values of  $Q/U_A$  show a strong correlation to what is expected from the previous computed results.

## SCALED RESIDUALS

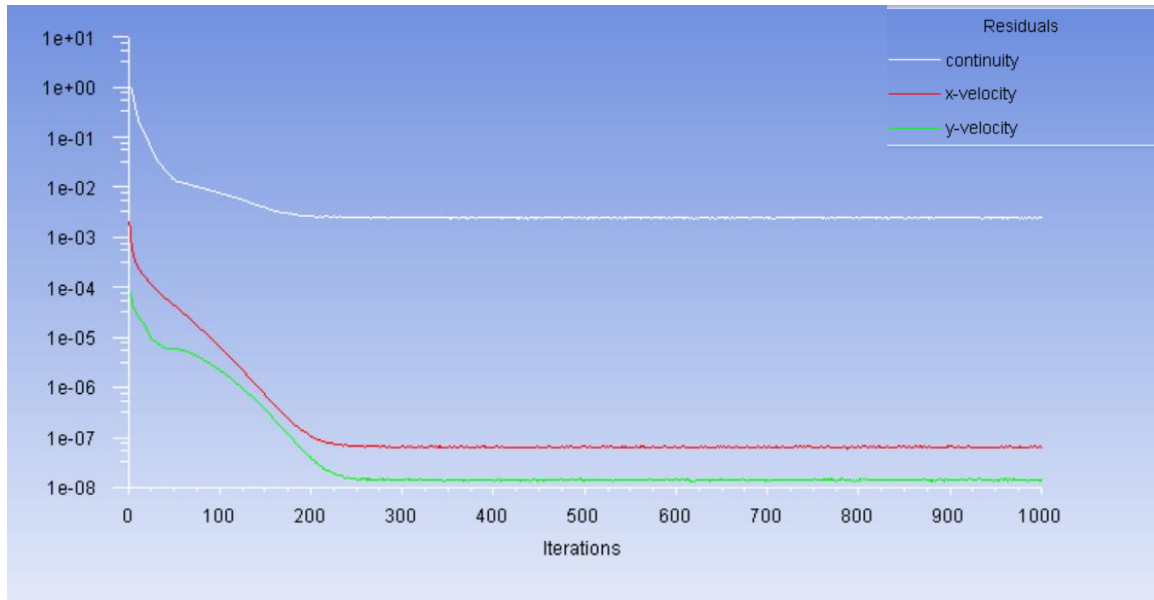


Figure 15: Figure showing scaled residuals for upstream velocity,  $U_\infty = 4.2\text{m/s}$ .

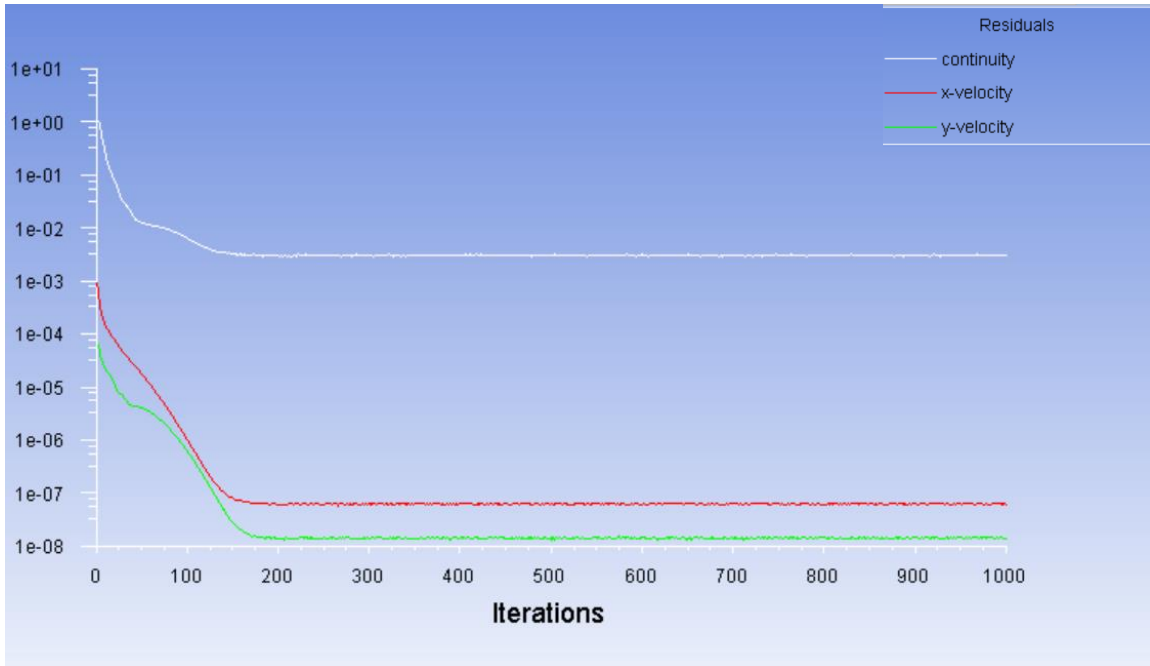


Figure 16: Figure showing scaled residuals for upstream velocity,  $U_{\infty} = 10.9 \text{ m/s}$ .

The figures for the scaled residuals for both  $U_{\infty} = 10.9 \text{ m/s}$  and  $U_{\infty} = 4.2 \text{ m/s}$ , show the convergence of the system at 1000 iterations. The values of continuity and the x and y components. There was an almost identical pattern for both velocities.

## FLOW PROPERTIES



Figure 17: Display of Velocity over the surface for the Validation of the Model provided by Skudarnov and Lin (2006)

The velocity Figure shown resembles closely the flow over a flat plate. It is interesting to note that there is a slight change in the velocity of the system at the point where the microbubbles are injected to the point where the fluid flows out of the system. The pressure outlet does not have any real effect on the system as the gauge pressure was assume to be constant, allowing the fluids to flow without any backflow in the system.

# FLOW OVER FLAT PLATE AT HIGH REYNOLDS NUMBER SETUP OF GEOMETRY

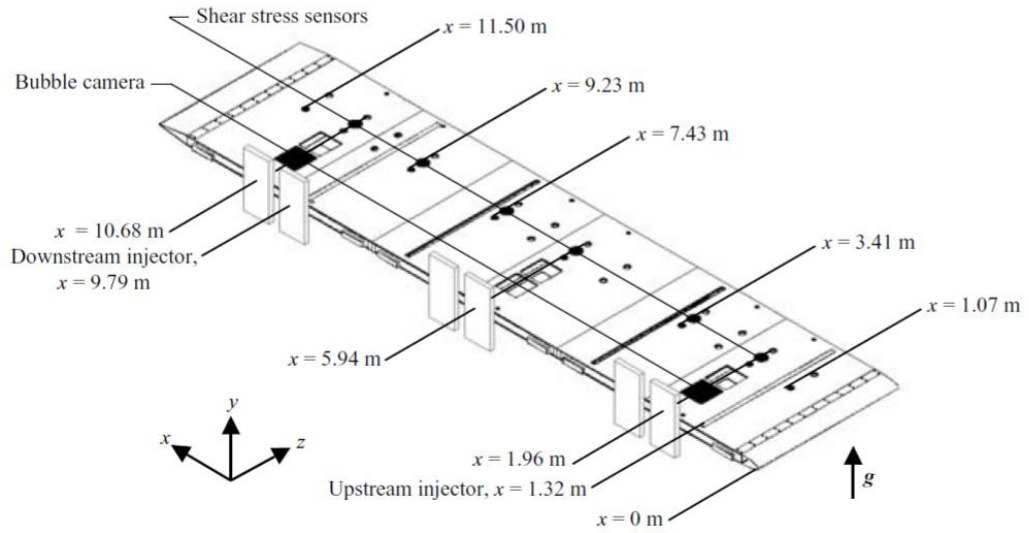


Figure 18: Schematic of the geometry setup for the case with flow over flat plate according to Wendy et al. (2006).

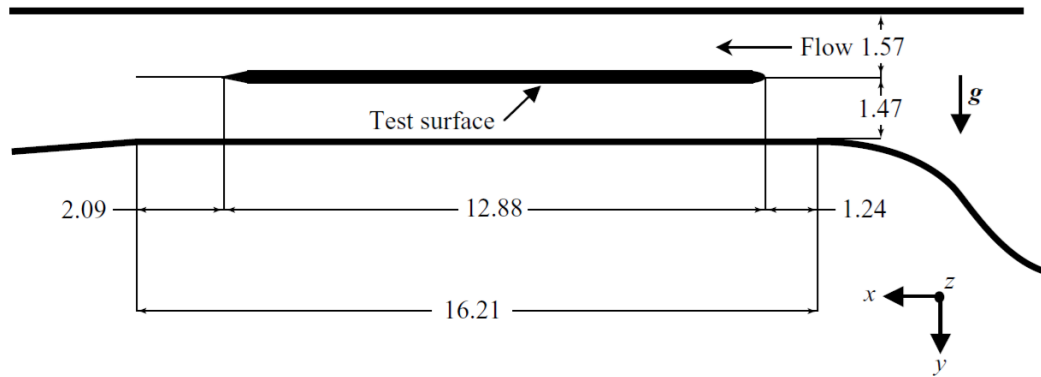


Figure 19: The cross-sectional view of the flat plate in the test tunnel which shows the dimensions to be used Wendy et al. (2006).

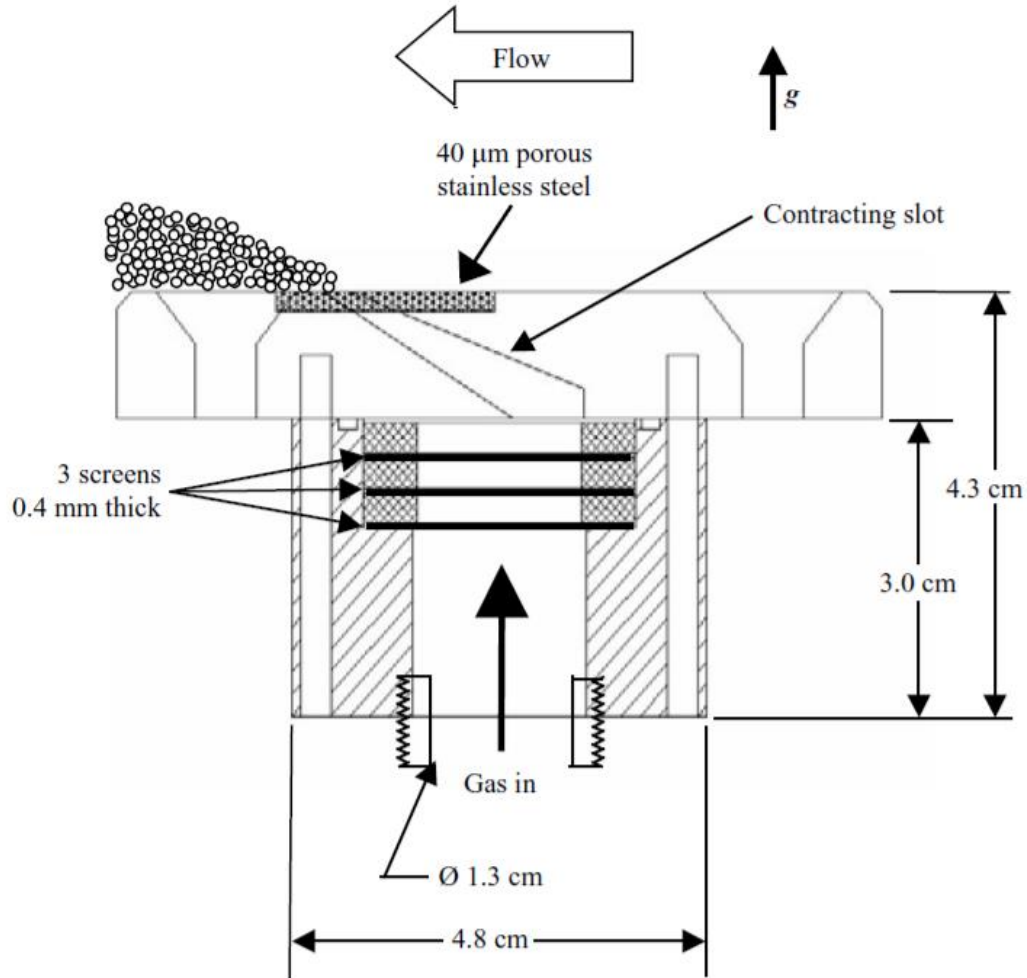
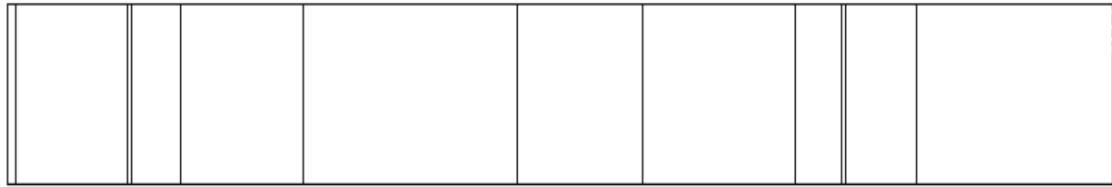


Figure 20: Enlarged view of the gas injection ports Wendy et al (2006).

For the case provided by Wendy et al. (2006), the geometry was setup in a manner that was identical to the description of the case provided. The system was setup so that it appears to be observed through a cross-sectional cut, with the dimensions shown in Figure 18 above. For the purpose of consistency in the simulations, the layout shown in Figure 19 is rotated  $180^\circ$  about the x-axis to appear up right. The height of the geometry was chosen to be  $1.47\text{m}$  per the details in Figure 19 and the length of each section was determined per the

dimensions shown in shown in Figure 7, which would give the locations for measuring the effect of drag. Each microbubble injection port shown in Figure 7 at  $x = 1.32m$  and  $x = 9.79m$  were created in as a separate plate area with a length of 4.8cm per the dimension shown in Figure 20. The display of the geometry was shown in Figure 21 below.



*Figure 21: The display of the setup of the geometry in ANSYS*

## **SETUP OF MESH, DETERMINATION OF SIZING AND MICROBUBBLE INJECTION ZONE**

The mesh was created to be consistent with the behavior of the mesh prescribed in Skudarnov and Lin (2006). The important mesh factors were to determine the number of cells and the resulting sizing such that the mesh would be able to capture changes in the flow and the boundary layer. An iterative procedure was used to determine the number of cells and bias factors that would be used so that a similar mesh sizing would ultimately appear throughout the system. The equations used were the same as those in the Flow over flat plate section. Additionally, a similar process was used to setup the first layer of cells over the walls designated as the source terms for the mesh to be manually created in these areas.

The mesh created was 500 X 200 and had a bias factor of 50 in the y direction and 20 in the x direction. The bias factors aided in the clustering of cells in the regions closet to the plate and in the transition zones between along the x-axis.

The equations used in the Flow over flat plate section was used here to determine the height of the first layer of cells to manually create the source term areas. The value of the height of the first layer of cells,  $a_{500}$  was found to be 0.0002m and the value of the new bias factor for the remaining cells over that zone,  $b_{499}$  was found to be 49.61. This information is summarized in Table 6 below.

Description	Symbol	Value	Unit
Overall height	$S_n$	1.47	m
Number of Cells	n	500	Dimensionless
Bias Factor	b	50	Dimensionless
Bias Factor new	$b_{499}$	49.61	Dimensionless
First Cell height	$a_{500}$	0.0002	m

Table 6: The values used for setting up the mesh sizing in ANSYS. This mesh was set up to analyze the case provided in the paper by Wendy et al. (2006).

Once the sizing of the mesh was determined, the mesh was created. The display of the mesh in ANSYS is seen in Figure 22 below. Figure 23 shows the location of the first cell in the mesh over one of the cell zones that were dedicated to be the source term and Figure 24 shows a close up view of the overall mesh shown in Figure 22 at the location of the transition between a designated source cell zone and the adjacent area.

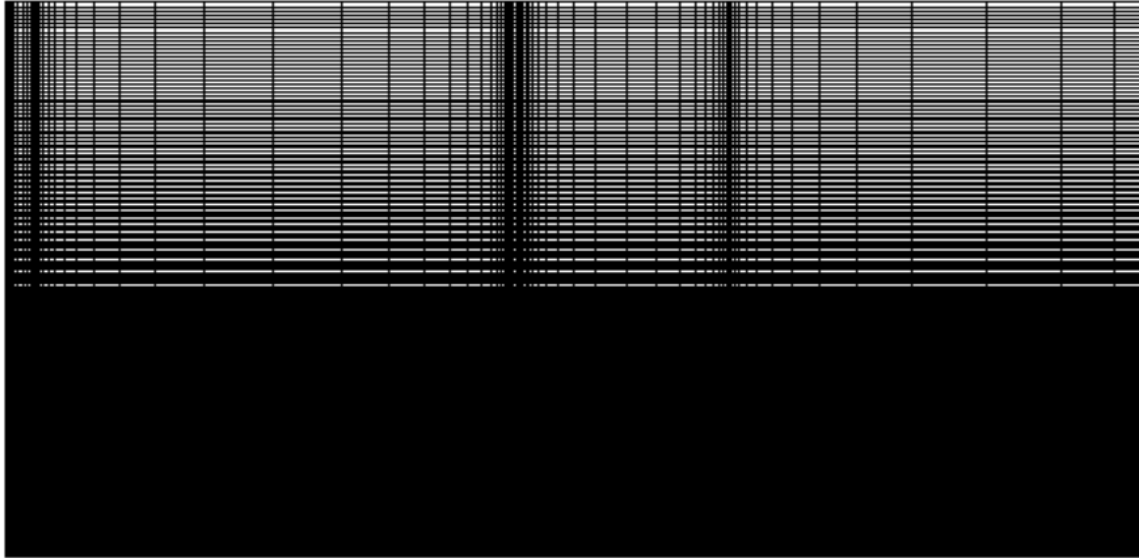


Figure 22: Extract from ANSYS showing the mesh used for the analysis for the extremely high Reynolds number case

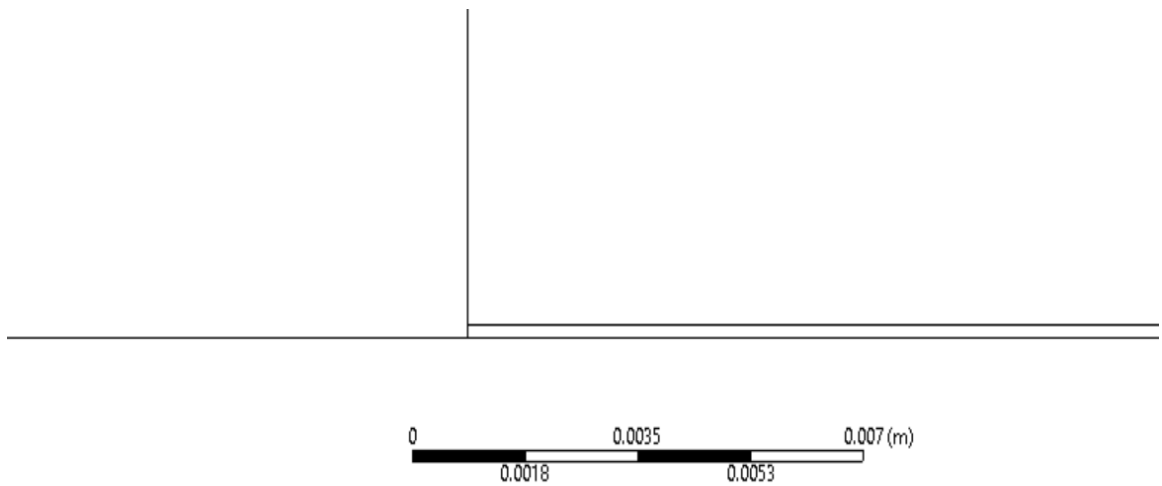
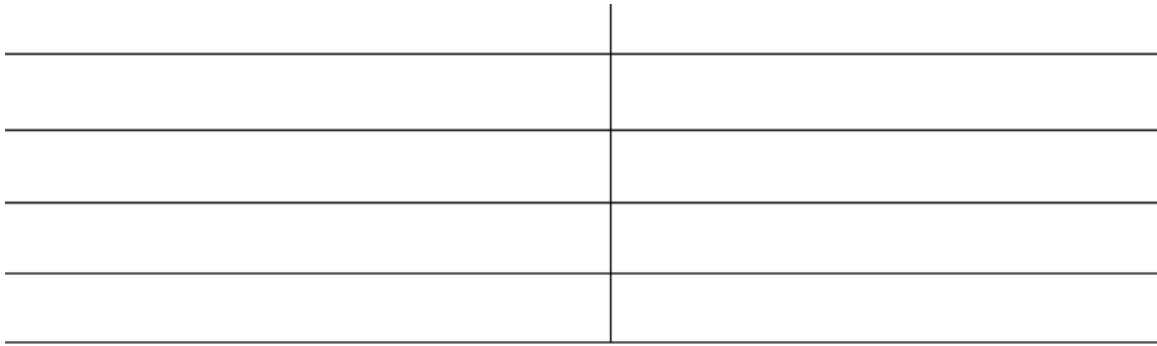


Figure 23: Depiction of the first layer of cells to be used as the source term for the extremely high Reynolds number case



*Figure 24: Enlarged View of the First layer of cells showing the seamless incorporation into the overall mesh for the extremely high Reynolds number case.*

## **SETUP OF SIMULATION MODELS**

The computational model was set up using the same modelling as Skurdanov and Lin (2006). Using the  $k$  and  $\omega$  model for the turbulence modelling and species transport to analyze the particles in the flow. In the model, the values of  $k$  and  $\omega$  were chosen as  $1.2 \times 10^{-5}$  and  $1.2 \times 10^{-3}$  respectively and these values were chosen for the initialization of the system. The species transportation in the modelling of the system was utilized to allow for the behavior of the gas to be correctly modelled.

## **MATERIALS SELECTION**

It was important that the materials be selected correctly to model the system. The material properties such as mass, density, and viscosity were important as they would be used in the computational model. The materials selected were Water (liquid) and Air for the mixture model which allowed for the model to accurately predict the behavior of the two fluids interacting as a mixture.

For the fluid zones; water was chosen as the carrier fluid and air to act as the injected microbubbles, these match the conditions prescribed by Wendy et al (2006).

### **CELL ZONE CONDITIONS**

Due to the setup of the model, there were three cells zones created. The two zones which were set to be the microbubble injected area, were assigned to be source terms for air. The remaining cell zone area was set as a fluid area.

### **BOUNDARY CONDITIONS**

The boundary conditions were set for the system as this was used extensively in the computational equations. The inlet was set as a velocity inlet boundary condition which used values of  $6 \text{ m/s}$ ,  $12 \text{ m/s}$  and  $18 \text{ m/s}$  which were consistent to the values used by Wendy et al (2006). Symmetry boundary conditions were used at the leading edge of the domain as well as the far field of the system which effectively predicts the behavior of the flat plate in a water channel. The no-slip boundary condition is applied to all walls which makes the plate act as a solid wall. The constant pressure boundary condition is applied at the outlet to ensure consistent flow. The initialization of the system used the inlet as the reference point which allowed the simulation to adopt the values of  $k$  and  $\omega$  as the initial guess.

### **ANALYSIS OF SIMULATION**

At the extremely high Re values the system was deemed to be valid per the information shown in Figure 36 to Figure 39, which compares both different

values of  $U_{\infty}$  and  $Q$ . It is interesting to note that both the model and observed results displayed dependence on distance along the x-axis for MBDR effectiveness. There was a consistent pattern of decreased performance the further away from the microbubble injection zone that the MBDR performance was observed.

## RESULTS

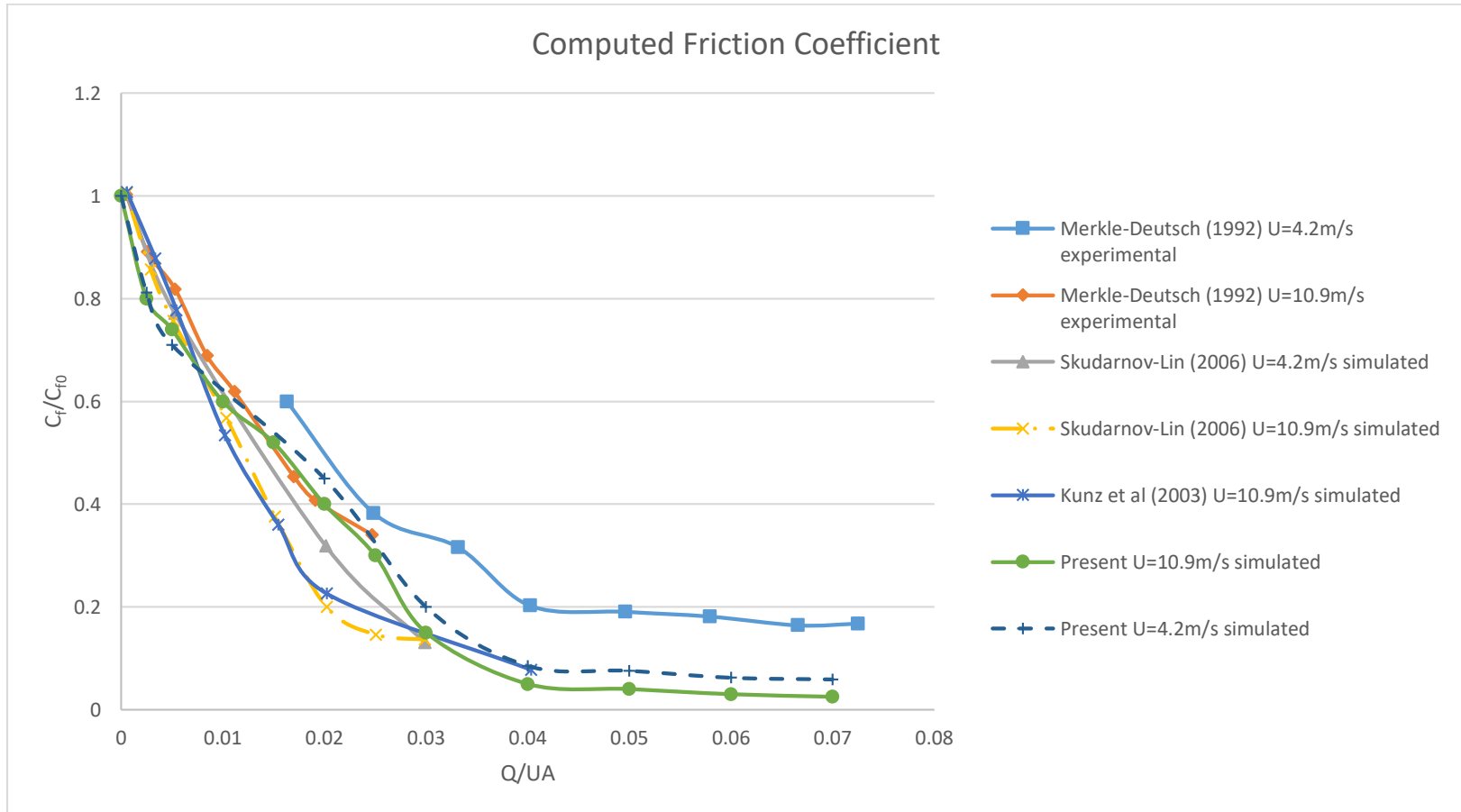


Figure 25: Computed Friction Coefficient - Comparison with Previous Results for Upstream Velocity  $U=10.9\text{m/s}$

Figure 25 gave the values of the computed friction coefficient for upstream velocity,  $U_\infty = 10.9 \text{ m/s}$  and  $U_\infty = 4.2 \text{ m/s}$ . This figure compares the experimental results by Merkle and Deutsch (1992), to the CFD analysis by Skudarnov and Lin (2006), Kunz et al. (2003) with the presently obtained results. This figure shows the effect of varying the gas injection rates while keeping all other factors constant. This result is for smooth surface with water as the fluid flowing and CO<sub>2</sub> microbubbles for the purpose of drag reduction. The results obtained shows a good agreement between the experimental results and the three sets of CFD analysis. This is interpreted as good support for the use of the CFD model as an accurate tool for predicting MBDR in this case.

As the gas injection rate increases the MBDR effect is increased, i.e. for increasing the value of non-dimensional flow coefficient,  $Q/U_A$ , the non-dimensional friction coefficient ratio,  $C_f/C_{f0}$ , decreases. This means that for higher gas injection rates,  $Q$ , the coefficient of friction decreases significantly over the surface. This is in agreement with the theoretical understanding of the mechanism of MBDR. Within a certain range of values, the MBDR effectiveness reduces quickly, however, as the value of microbubble injection rates increases very high the value of the drag reduction gradually began sloping to approximately 98% MBDR effectiveness values. This is a similar occurrence to what was obtained from the experimental results .

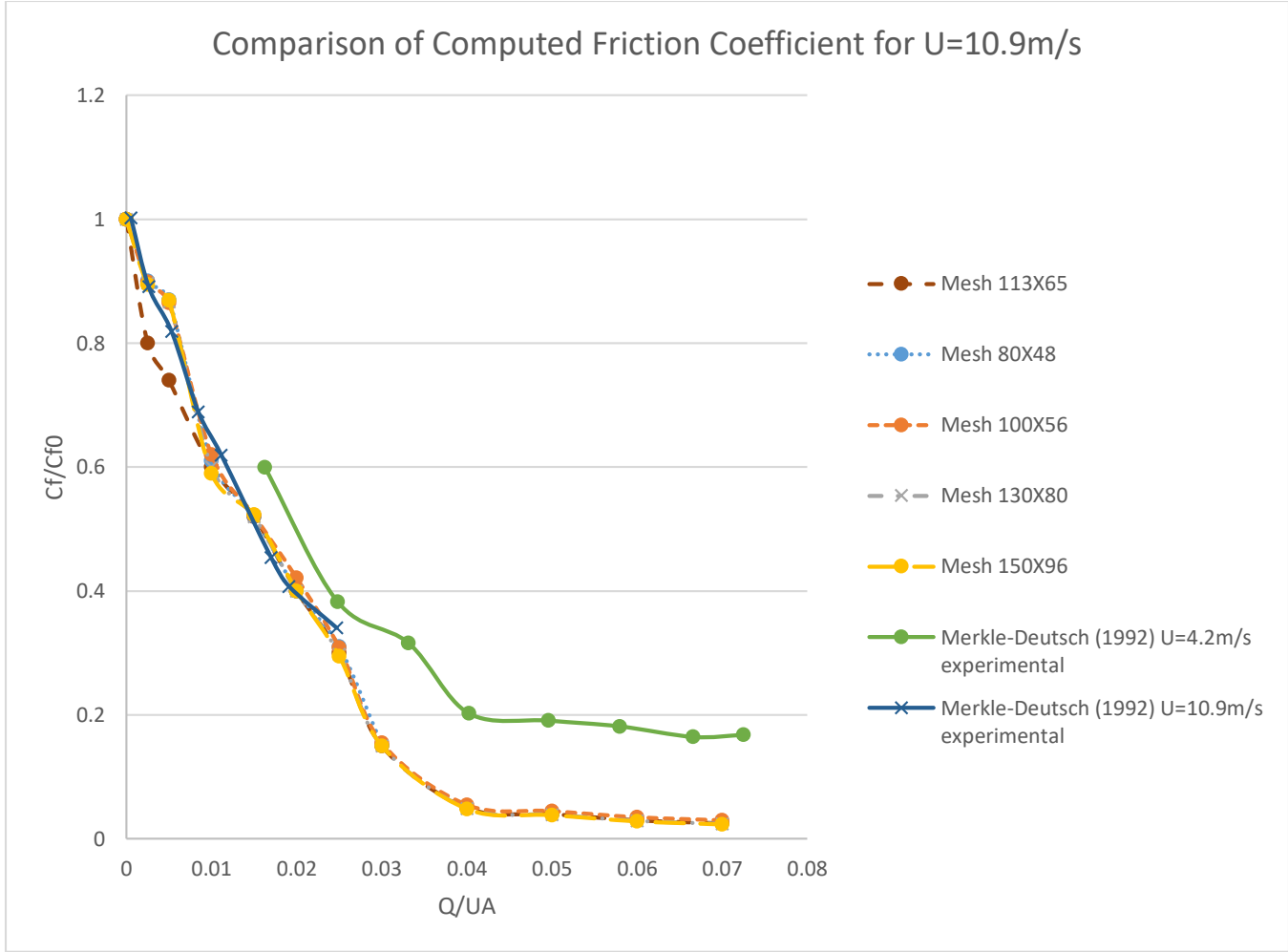


Figure 26: Comparison of Computed Friction Coefficients for different mesh sizes at U=10.9m/s

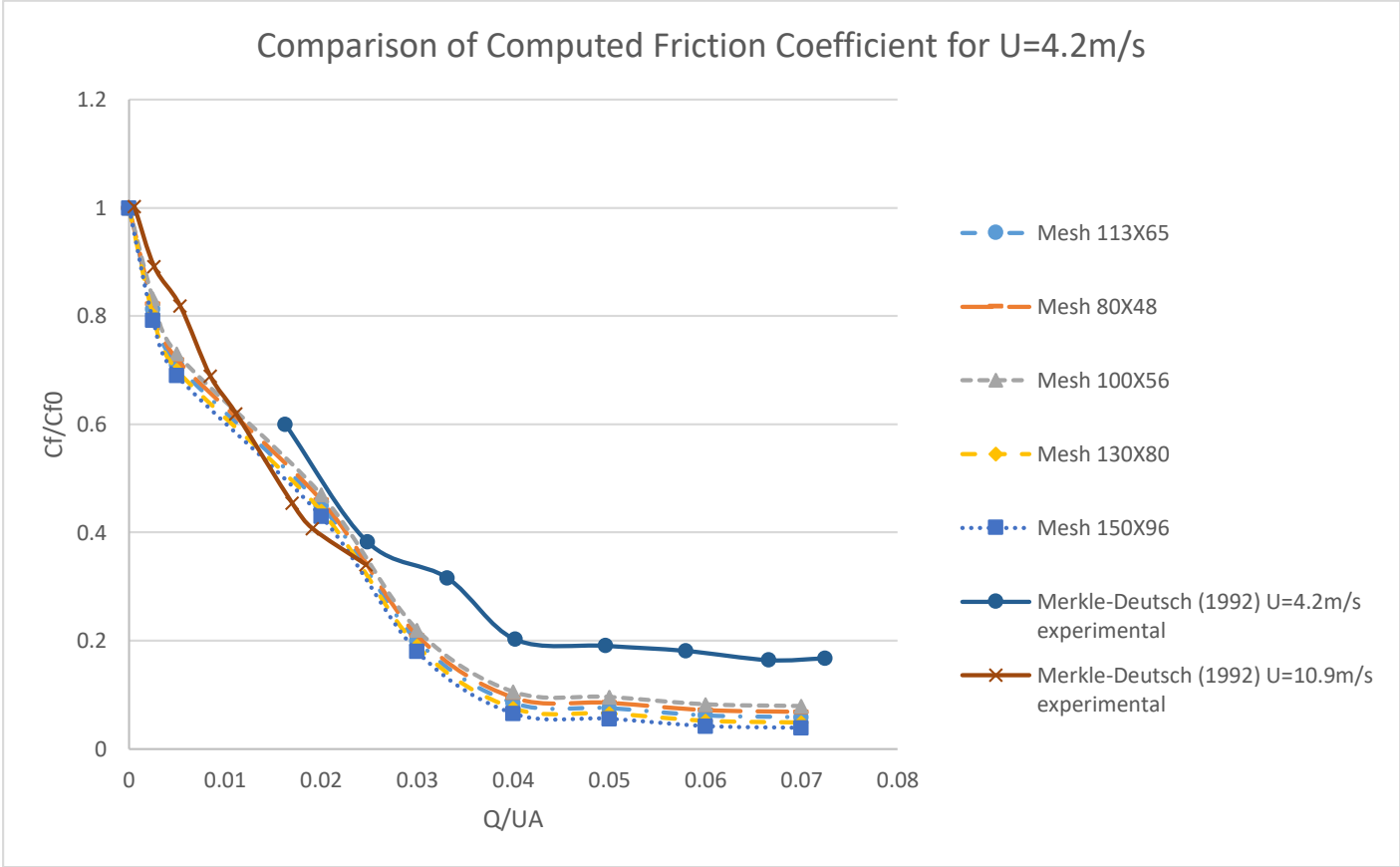


Figure 27: Comparison of Computed Friction Coefficients for different mesh sizes at U=4.2m/s

It was of interest to determine the difference in the behavior of the model when subjected to different mesh sizing. There were two coarser mesh sizes set up, two finer mesh sizes set up and the initial 113X65 mesh was used as well, giving a total of five mesh sizes which were used to carry out a mesh dependence study. It was found that there was no mesh dependence on the model for the study. The results remained the same for both  $U_{\infty} = 4.2 \text{ m/s}$  and  $U_{\infty} = 10.9 \text{ m/s}$ . This is clearly seen in Figure 26 and Figure 27, where the simulated results basically fall one a top each other. The values still vary from the results obtained in the CFD analysis by Skudarnov and Lin (2006), however, the model can be considered correct due to it being mesh independent.

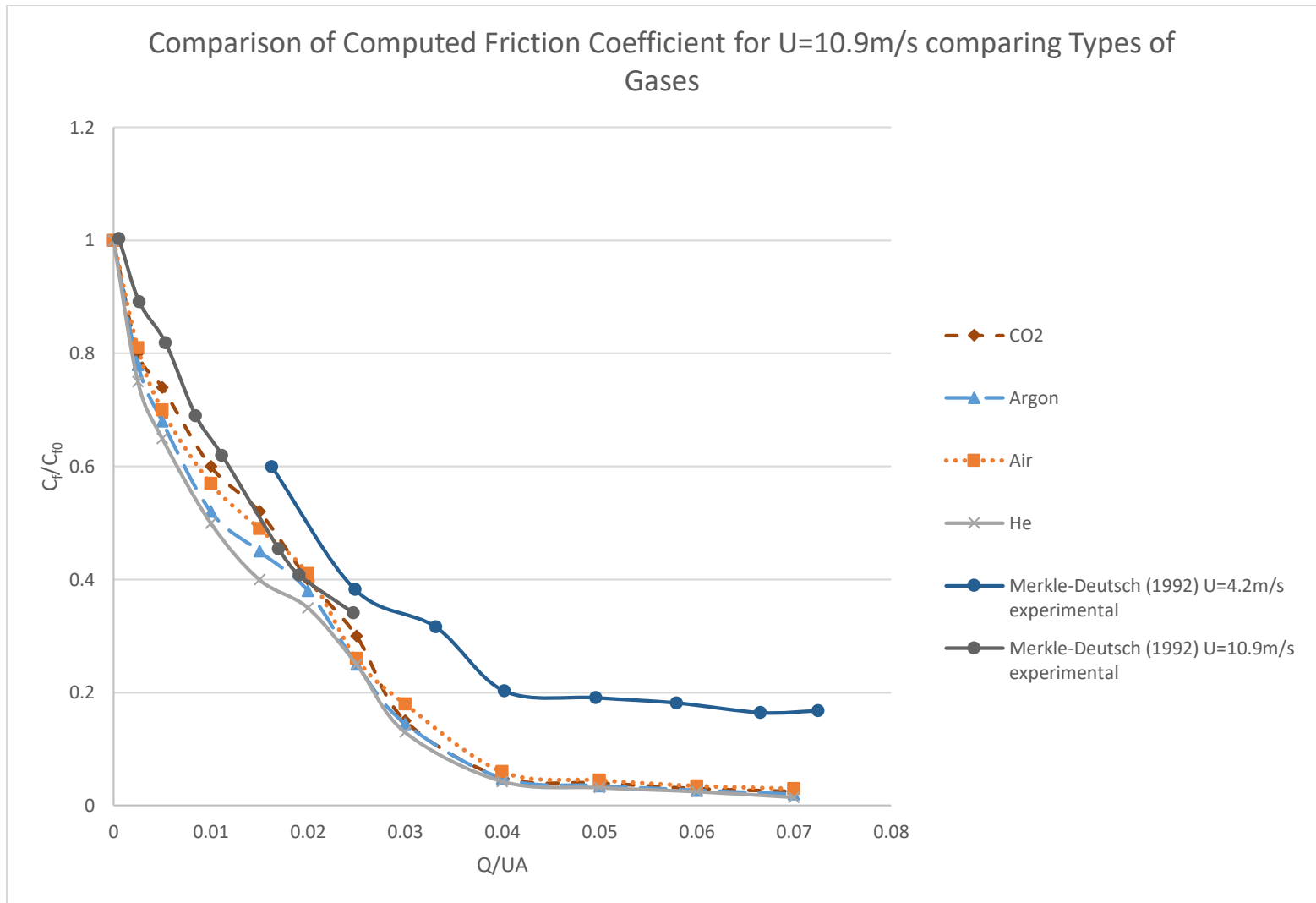


Figure 28: Comparison of Different Gases acting as the source of microbubble injection for U=10.9m

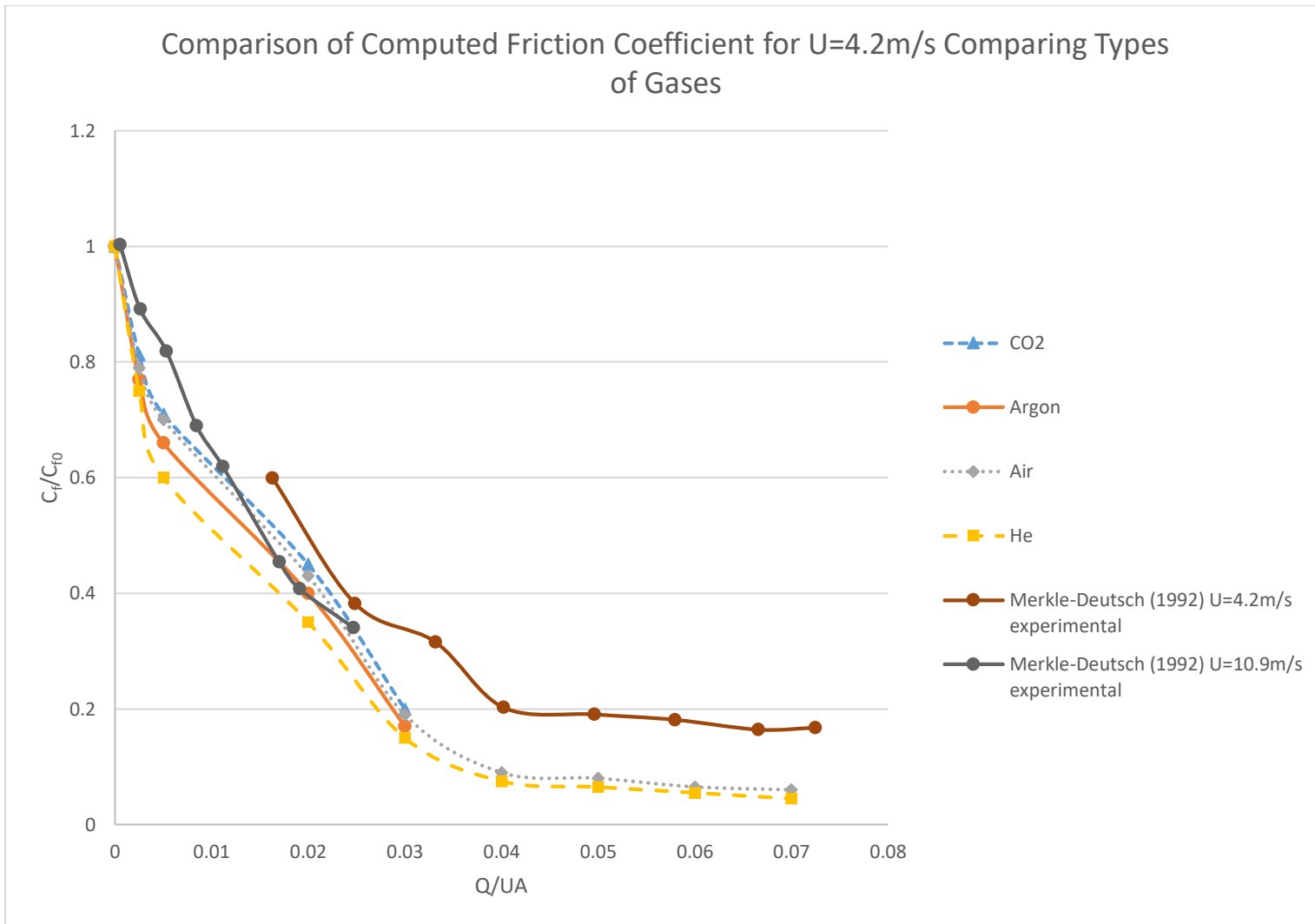


Figure 29: Comparison of Different Gases acting as the source of microbubble injection for U=4.2m/s

The results displayed in Figure 28 and Figure 29 display the effect of different gases on MBDR for upstream velocity,  $U_{\infty} = 10.9 \text{ m/s}$  and  $U_{\infty} = 4.2 \text{ m/s}$  respectively. The intent was to compare this work with the previous experimental results by Deutsch et al (1992). In that work, it was found that as the gases used for the microbubble injection changed there was a change in the MBDR capability of the system. The findings was such that as the density of the injected gas decreased the MBDR capability increased. For determining the behavior, the set up by Skudarnov and Lin (2006) was used to perform the simulation and the gases were varied. The gases used were those used by Deutsch et al (1992), and listed in descending order of density ratio values: helium, air, argon and carbon dioxide.

The results obtained showed a behavior of the system that has strong agreement with the experimental results. Theoretically, the higher the density ratio (DR) the better the MBDR capabilities of the system. In this figure it is clear that helium has the best MBDR capability, followed by air, argon and carbon dioxide in descending order of MBDR effectiveness. It is important to note that the difference in the MBDR effectiveness across the gases were very small. The interpretation of these results were found to be consistent with the experimental findings of Deutsch et al (1992) and the simulated results of Skudarnov and Lin (2005), where the MBDR effectiveness was inversely proportional to DR. The comparison of these results gave a concrete understanding of the effect of different gases on MBDR and its ability to be used in the model.

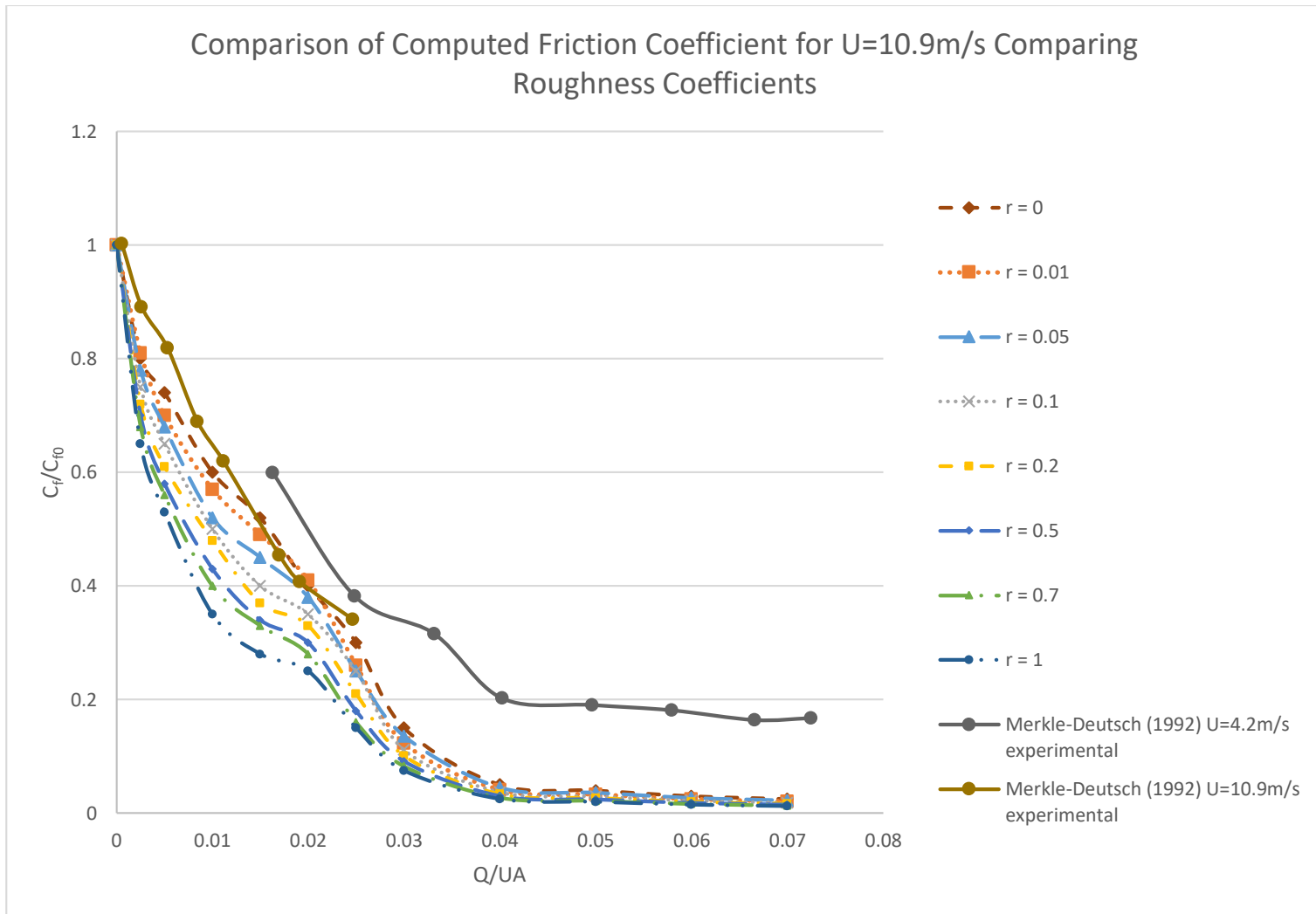


Figure 30: Comparison of Roughness to Ratio of Drag Reduction for U=10.9m/s

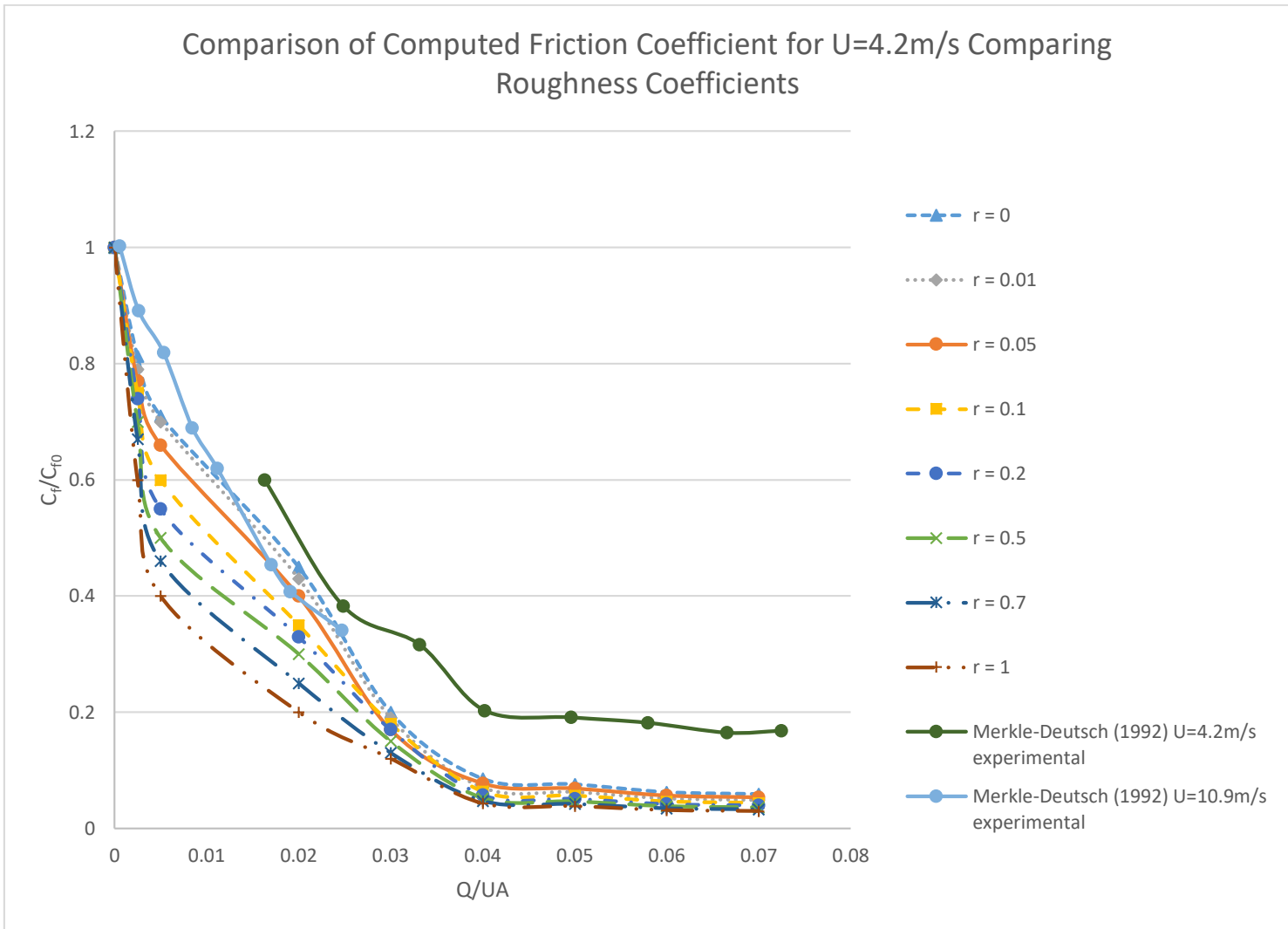


Figure 31: Comparison of Roughness to Ratio of Drag Reduction for U=4.2m/s

Figure 30 and Figure 31 display the results for the effect of wall roughness on MBDR for  $U_\infty = 10.9 \text{ m/s}$  and  $U_\infty = 4.2 \text{ m/s}$  respectively. The present results were used to validate the behavior of the system and comparing to the conclusions obtained in experimental results carried out by Deutsch et al (2004). Based on his findings, the increase in roughness coefficient increases the MBDR effectiveness. Using flow over a flat plate, the present paper sought to validate the findings with CFD.

It was found that the model was able to accurately predict the behavior of the system with changing roughness coefficients. For the case where roughness coefficient,  $r = 0$ , this was taken as the control case and is the case that was used throughout the study. It was clear that as the values of  $r$  increased the MBDR effectiveness increased as well. It was found that for the CFD analysis, the difference between the lowest values of roughness coefficient,  $r = 0$ , and the highest,  $r = 1$ , there was approximately 35% improvement in drag reduction capabilities. This figure can be somewhat deceiving. The MBDR effectiveness was measured through the use of the non-dimensional value,  $C_f/C_{f0}$ . This gives the ratio between the skin friction coefficient,  $C_f$ , for a particular value of microbubble injection,  $Q$ , to the skin friction coefficient,  $C_{f0}$ , for the case without microbubbles. It was noted in Deutsch et al (2004), and in the present analysis that the skin friction coefficient,  $C_f$ , may be increased with roughness for values of  $Q$ , although the MBDR effectiveness increased.

The confirmation of the model to be used as an effective analysis for MBDR with roughness was important. The importance is underlined in the fact there hasn't been extensive CFD analysis to confirm the behavior of roughness with MBDR. The validation of the roughness effect in MBDR with the present results, serves both to further validate accuracy of the model and validate the results produced by experimentally.

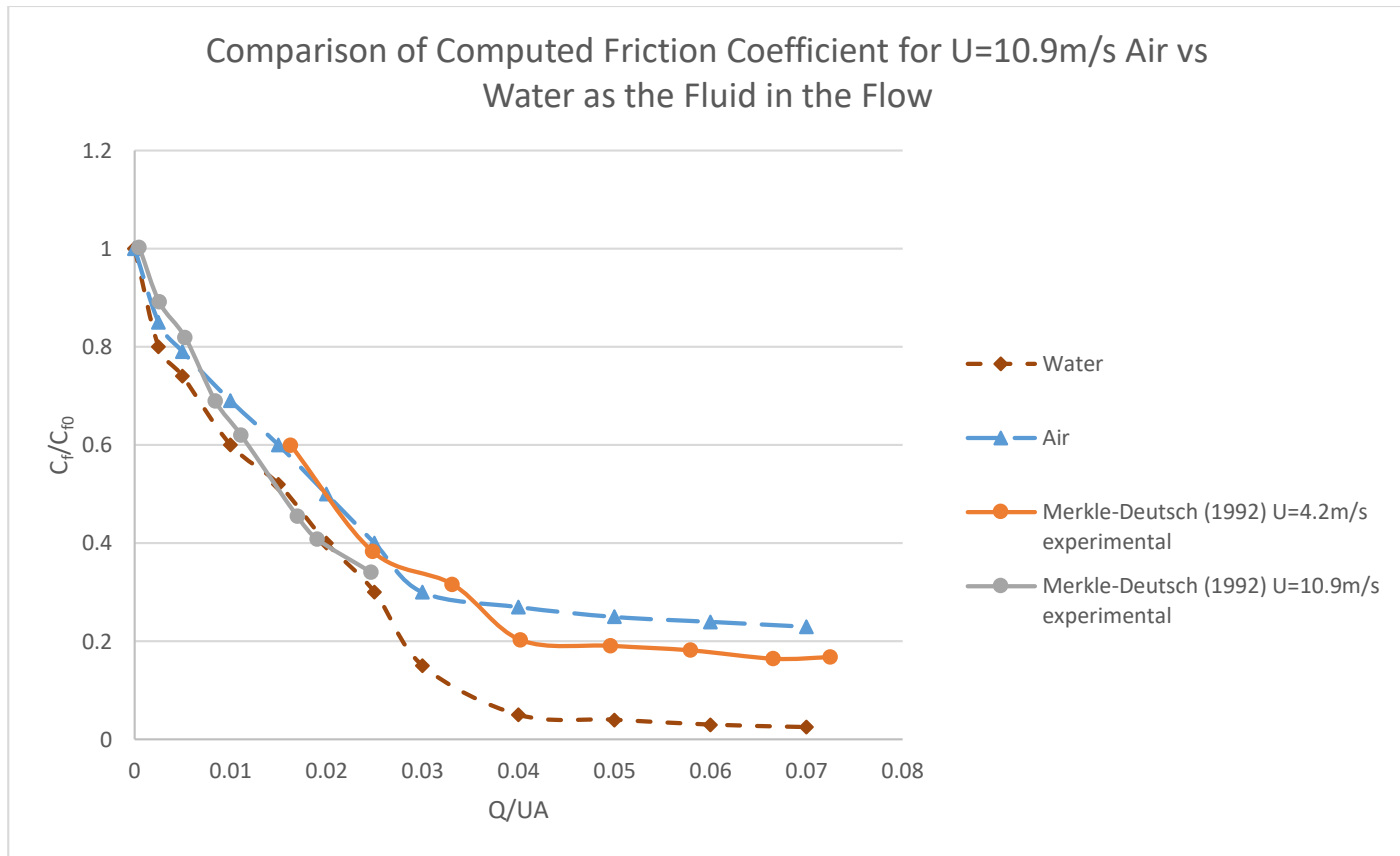


Figure 32: Comparison of Air vs Water as the Fluid in the free stream with CO2 microbubbles being injected for upstream velocity at 10.9m/s

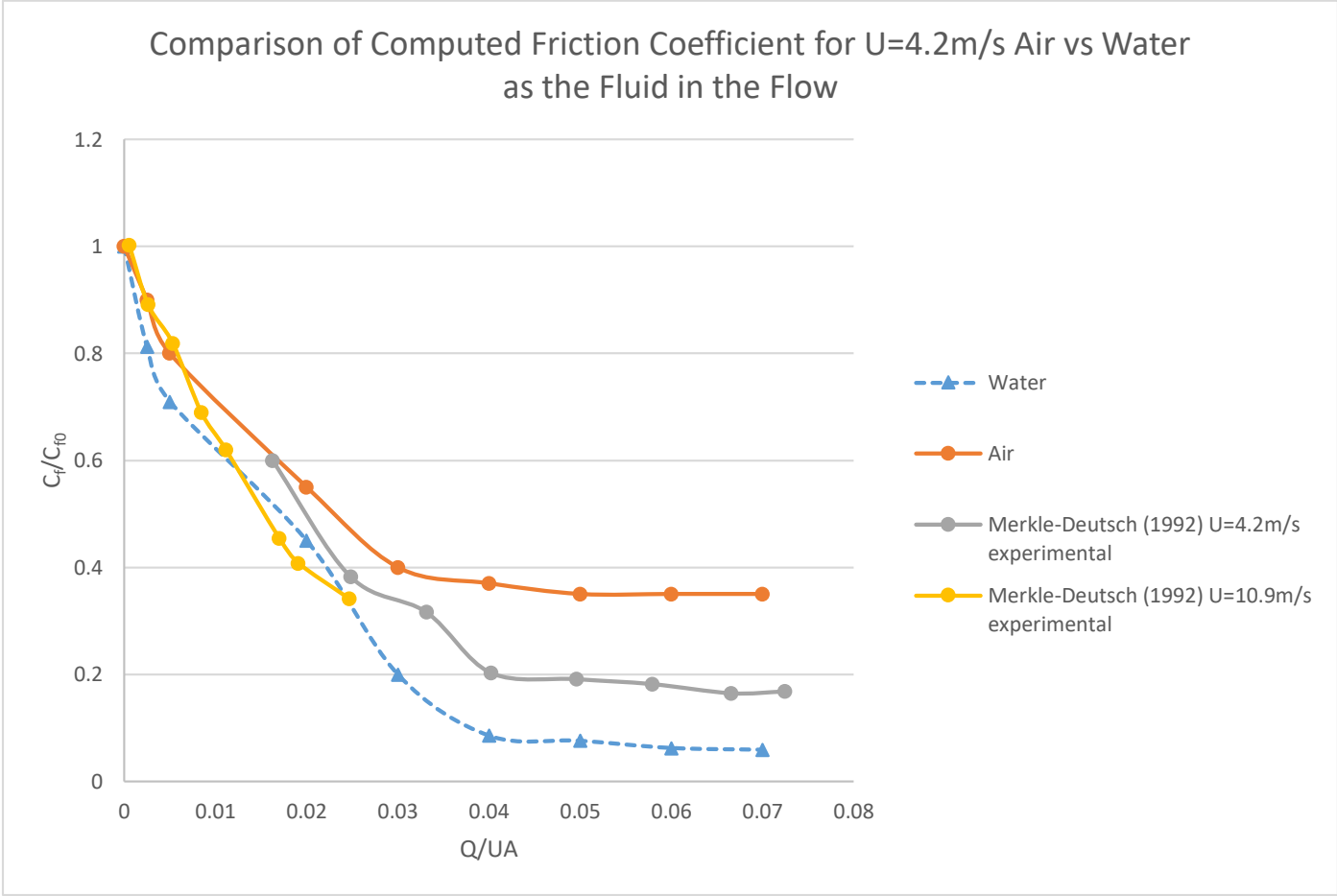


Figure 33: Comparison of Air vs Water as the Fluid in the free stream with CO2 microbubbles being injected for upstream velocity at 4.2m/s

Figure 32 and Figure 33 display the results for the effect of changing the upstream fluid on MBDR for upstream velocities,  $U_{\infty} = 10.9 \text{ m/s}$  and  $U_{\infty} = 4.2 \text{ m/s}$ . For these cases, air and water were interchanged as the upstream fluid. This is a concept that has limited if any previous results. The change in upstream fluids, particularly using a gas as the upstream fluid opens new applications for MBDR. Typically, MBDR has been used mainly between a liquid and gas. This use of air as the upstream fluid, gives results similar to what was expected from the understanding of MBDR, i.e. the effectiveness of MBDR is dependent on the density ratio (DR). This shows that it is possible for MBDR to occur in systems with gases as well as liquids. This can open avenues for the for MBDR applications to new industries.

The effectiveness of MBDR was less for air than for water due to the lower DR. The MBDR effectiveness for air was very close to the values of water up to the values of about  $Q/U_A = 0.02$ . At this point the results deviate from each other with water having much higher MBDR effectiveness while the effectiveness for that of air remained relatively constant, meaning that there is an optimal value for MBDR to occur in systems with only gases. It is important to note that similar behavior was observed for both upstream velocities which means that the results can be taken as verified. It is suggested that a secondary validation be performed which incorporates experimental results for the use of MBDR in cases where air is the fluid.

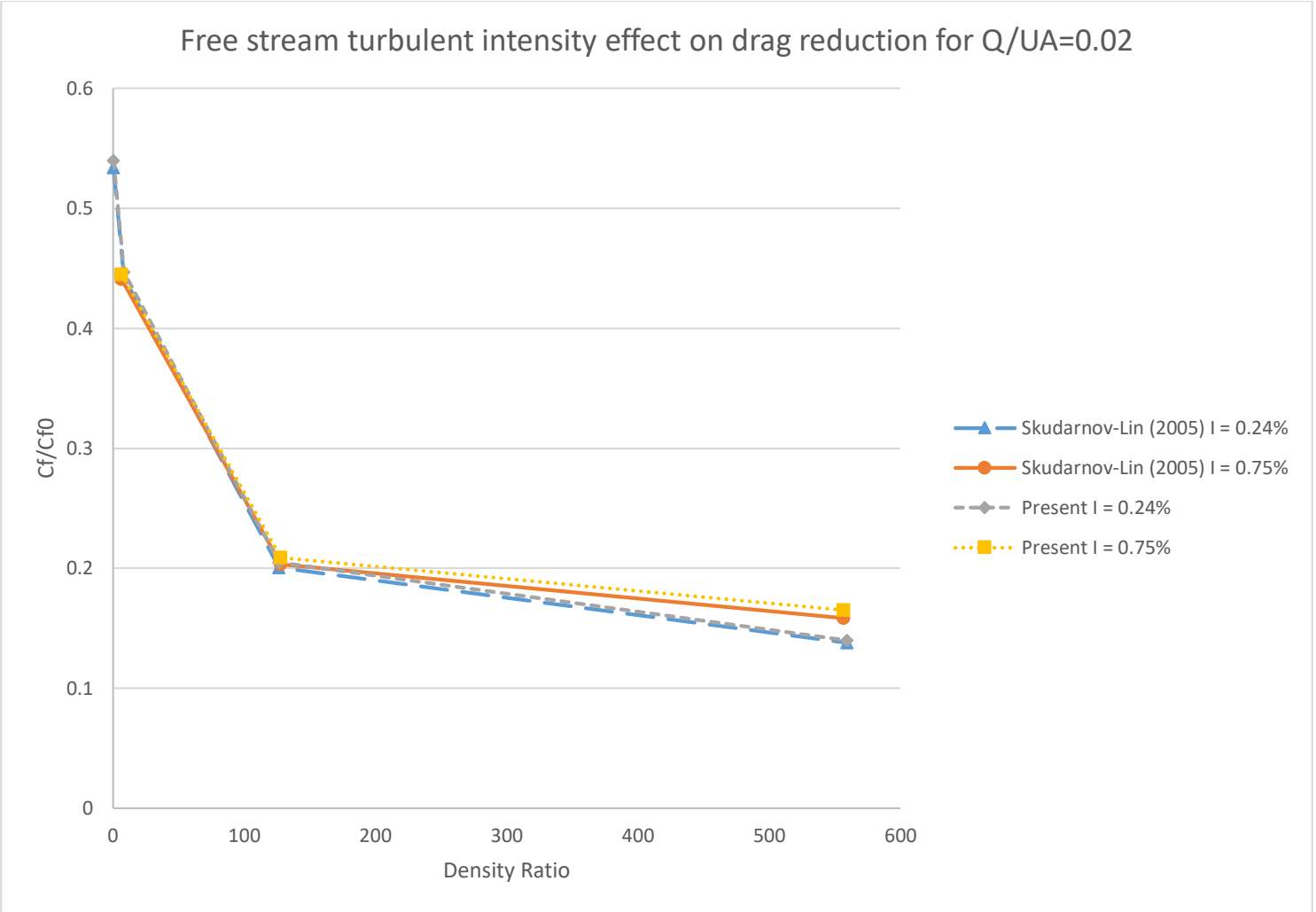


Figure 34: Free stream turbulent intensity effect on drag reduction for  $Q/UA=0.02$ .

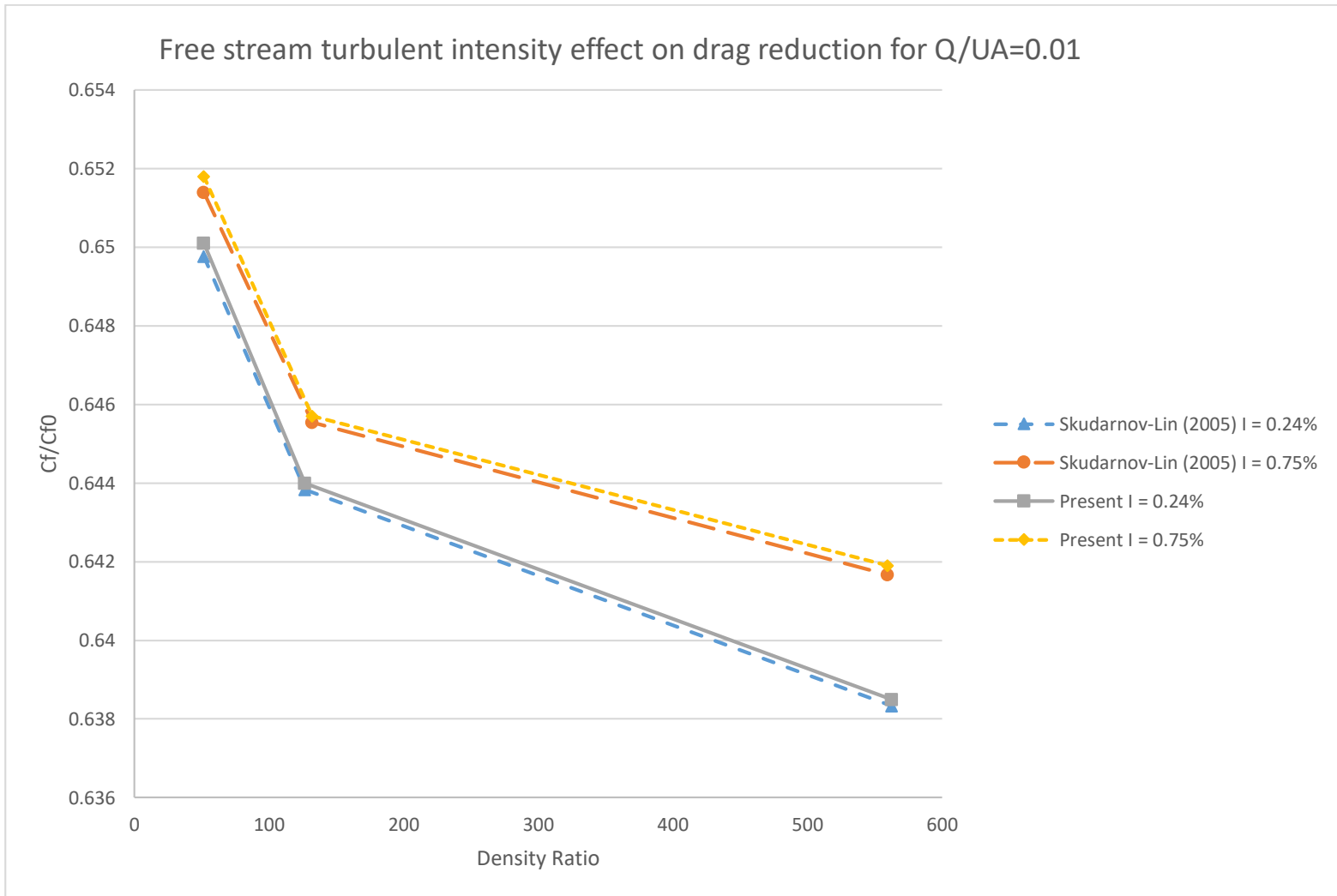


Figure 35: Free stream turbulent intensity effect on drag reduction for  $Q/UA=0.01$

Figure 34 and Figure 35 show the effect of the intensity ratio on MBDR. This was validated and compared against the values obtained from Skudarnov and Lin (2005), which used CFD analysis to compare the effect of turbulent intensity on MBDR. The analyses were performed for  $Q/UA = 0.02$  and  $Q/UA = 0.01$ , shown in Figure 34 and Figure 35 respectively. It was found that as the turbulent intensity at the inlet decreased the effectiveness of the MBDR increased. Additionally, it was also confirmed that as the density ratio increased the effectiveness of MBDR.

The behavior of the present model was almost exact to that of the one used by Skudarnov and Lin (2005). The difference between the results produced by both models were approximately 1% for both  $I = 24\%$  and  $I = 75\%$  for  $Q/UA = 0.01$ . For  $Q/UA = 0.02$  the difference for  $I = 24\%$  was approximately 2% and for  $I = 75\%$  the difference was 4%. This shows very good agreement between the present results and those previously obtained. This further validated the effectiveness of the model.

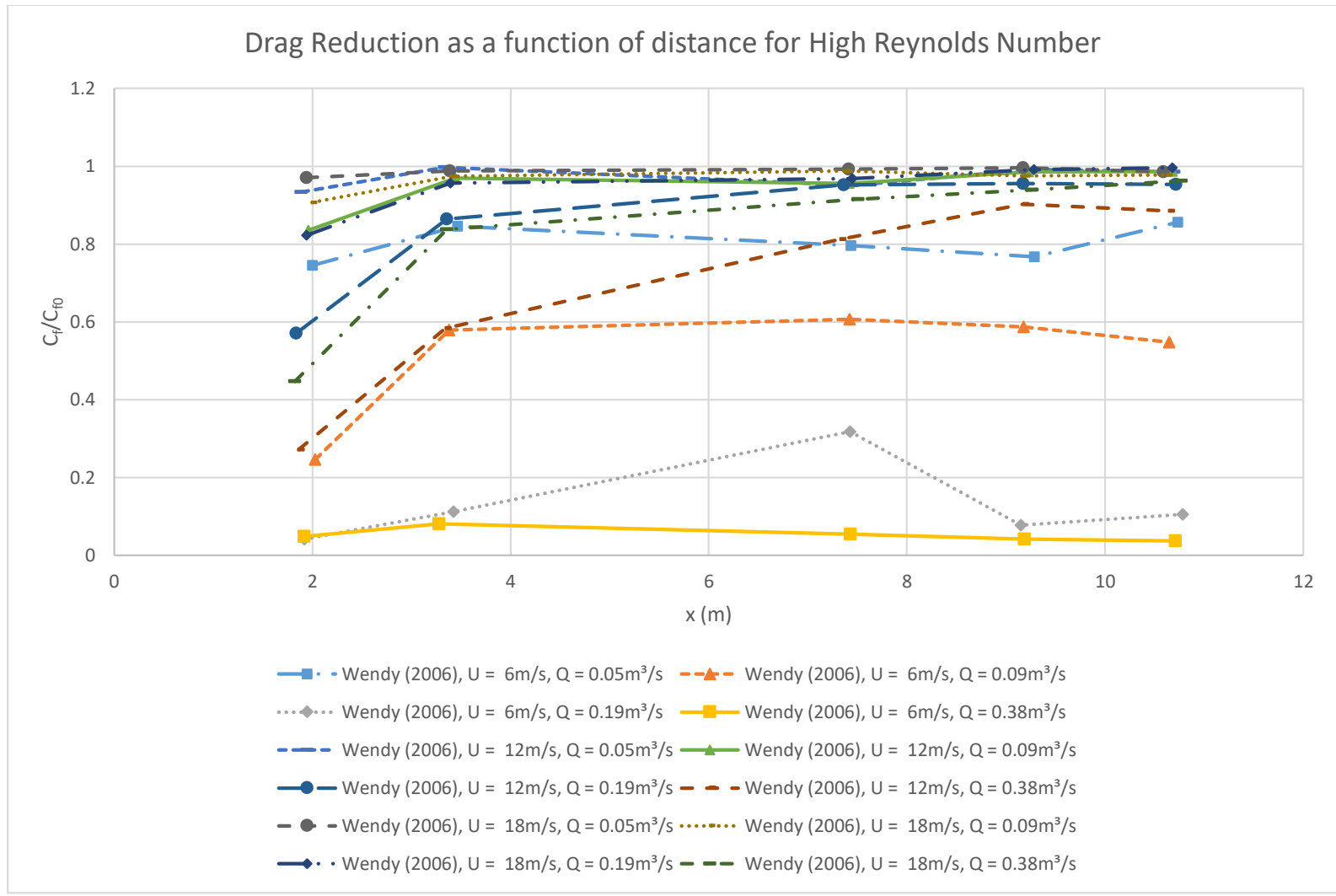


Figure 36: Comparison of Microbubble Drag Reduction as a Function of Distance for High Reynolds Number. This is a summary of the experimental Results

Figure 36 shows the behavior of drag reduction over distance for high Re. This was compared with experimental values obtained by Wendy et al. (2006). That study was conducted by using flow over a flat plate and setting up strain sensors at several points downstream of the flow. Additionally, there was an upstream and downstream source of microbubble injection. This paper found that the effectiveness of MBDR was highest at the zones nearest the source of the microbubbles.

The study was performed using values of the upstream velocity of  $6 \text{ m/s}$ ,  $12 \text{ m/s}$  and  $18 \text{ m/s}$ . The gas injection rates,  $Q$ , were also manipulated using values of  $0.05 \text{ m}^3/\text{s}$ ,  $0.09 \text{ m}^3/\text{s}$ ,  $0.19 \text{ m}^3/\text{s}$  and  $0.38 \text{ m}^3/\text{s}$ . For the lowest velocity,  $6 \text{ m/s}$  and highest value of  $Q$ ,  $0.38 \text{ m}^3/\text{s}$ , the highest effectiveness MBDR was observed due to the fact the microbubbles were able to form a gas film on the surface (Wendy et al., 2006). Additionally, the high MBDR effectiveness near the injection zones was due to the fact that the microbubbles were closer to the surface in these areas before they were able to disperse into the surrounding flow. It can be seen that as the upstream fluid velocity increases the effectiveness of MBDR decreases.

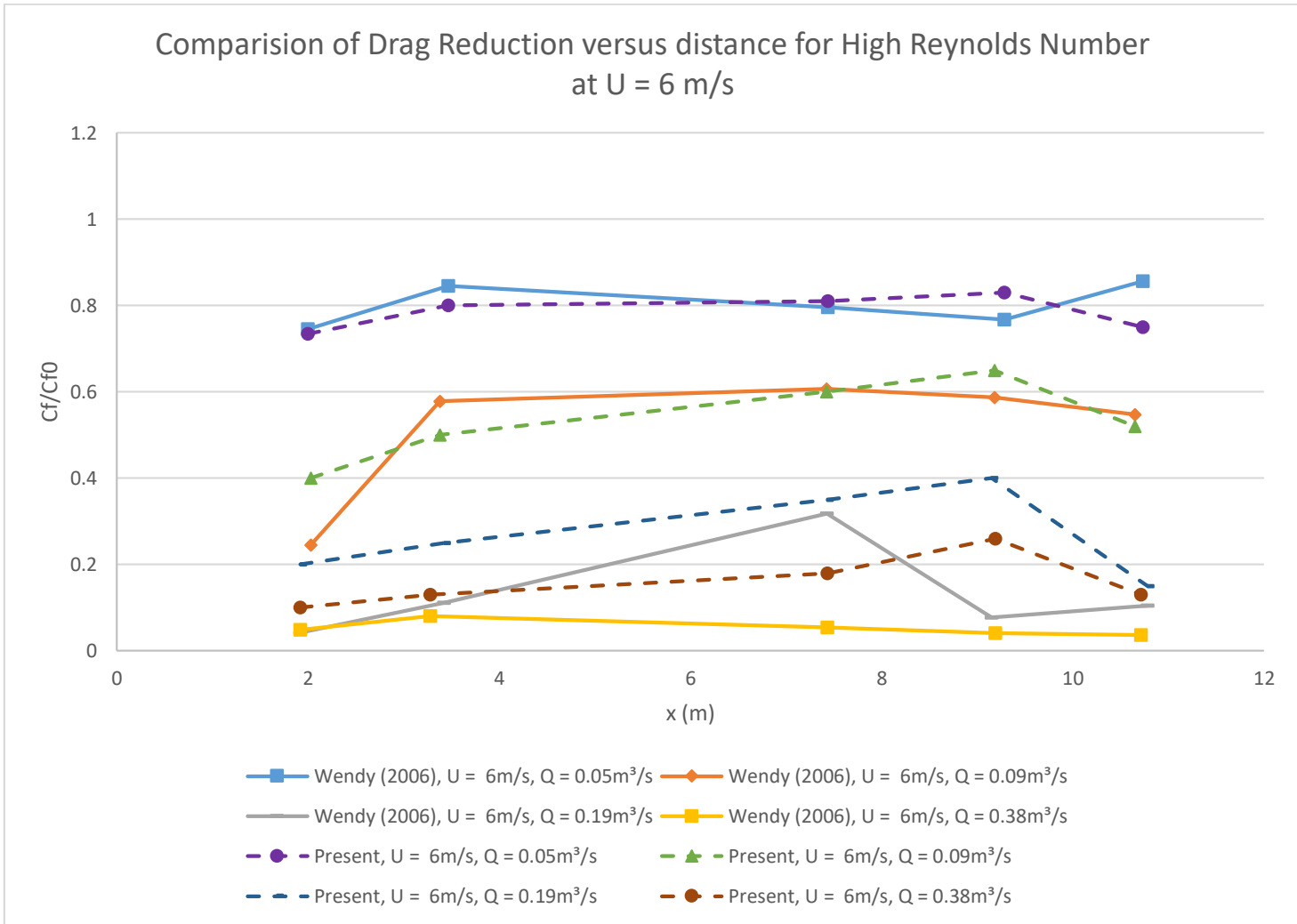


Figure 37: Comparison of Drag Reduction versus distance for High Reynolds Number at  $U = 6 \text{ m/s}$

Figure 37 compares the behavior of the experimental results by Wendy et al. (2006) and present simulations. The case in this figure was for  $U_{\infty} = 6 \text{ m/s}$ , while using varying values of Q. For this simulation, a similar effect was obtained for both the experimental results and those obtained by the simulations. The simulations found that MBDR effectiveness was dependent on the downstream distance. There was also agreement between the simulations and the results that MBDR was dependent on values of gas injection rates. It was validated that for high Re, as the value of Q increases, the MBDR effectiveness increases. This validates the fact that MBDR is dependent on the velocity of the inlet flow and microbubble gas injection rate. The good correlation between the experimental and simulated results validate that the model can be used at high Re cases. In this case the differences between the experimental and simulated results was on average, approximately 30%, which can be attributed to human error in the experiments.

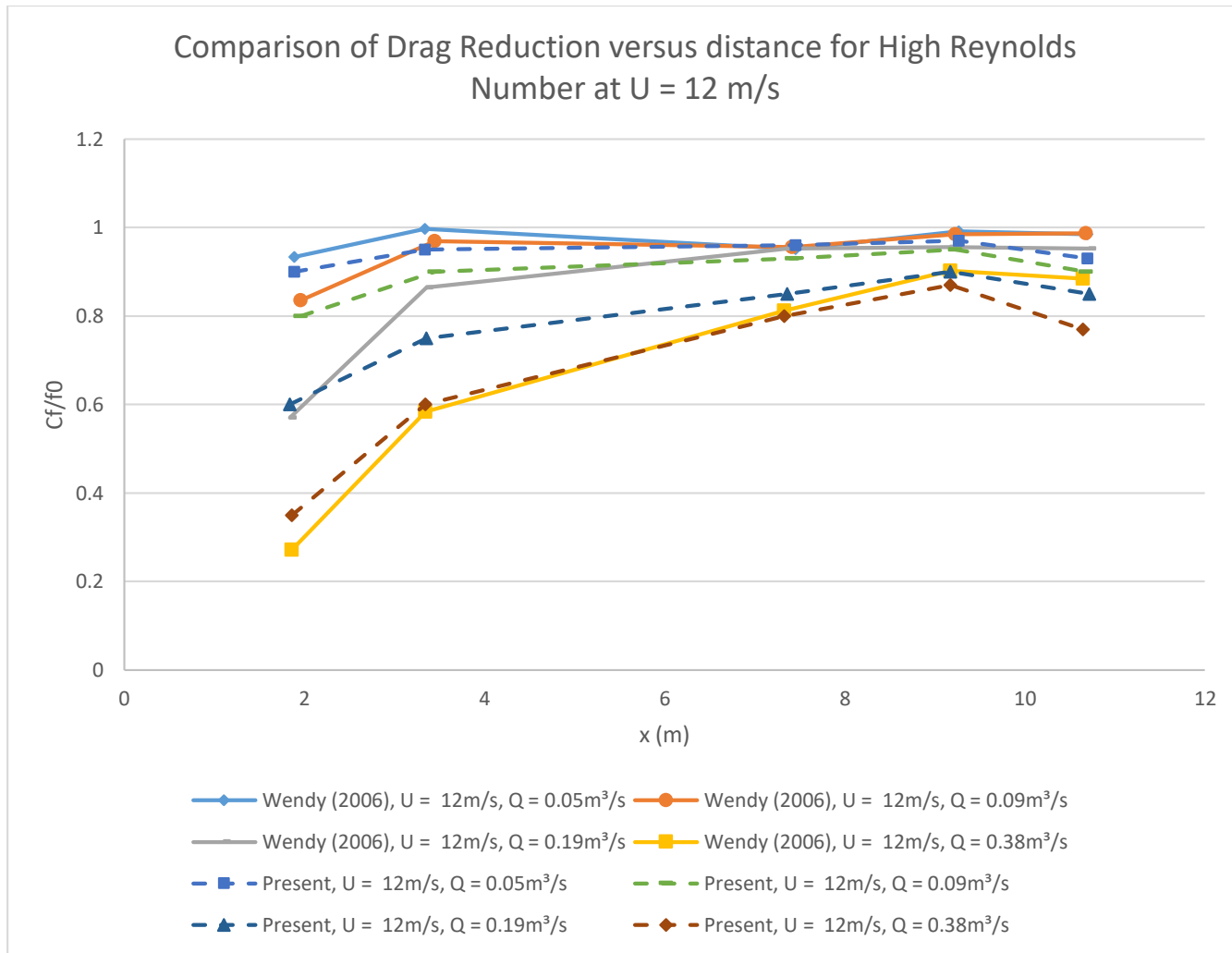


Figure 38: Comparison of Drag Reduction versus distance for High Reynolds Number at  $U = 12 \text{ m/s}$

Figure 38 compares the behavior of the experimental results by Wendy et al. (2006) with the present simulations for  $U_\infty = 12 \text{ m/s}$ , while varying all values of  $Q$ . Both sets of results found that MBDR effectiveness was dependent on distance and gas injection rates,  $Q$ . The performance of the MBDR was found to be not that effective with distance for this high  $Re$ . One reason for this effect could be that the microbubbles would not be able to create the film surface effectively under the high  $Re$  conditions, basically having the microbubbles blown away by the flow. It is important to note that increased performance was found for higher flow rates of microbubbles, which validates the fact that MBDR is dependent on the microbubble gas injection rate. The good correlation between the experimental and simulated results validate that the model can be used at high  $Re$  cases. The average difference between the experimental and simulated values were approximately 6%.

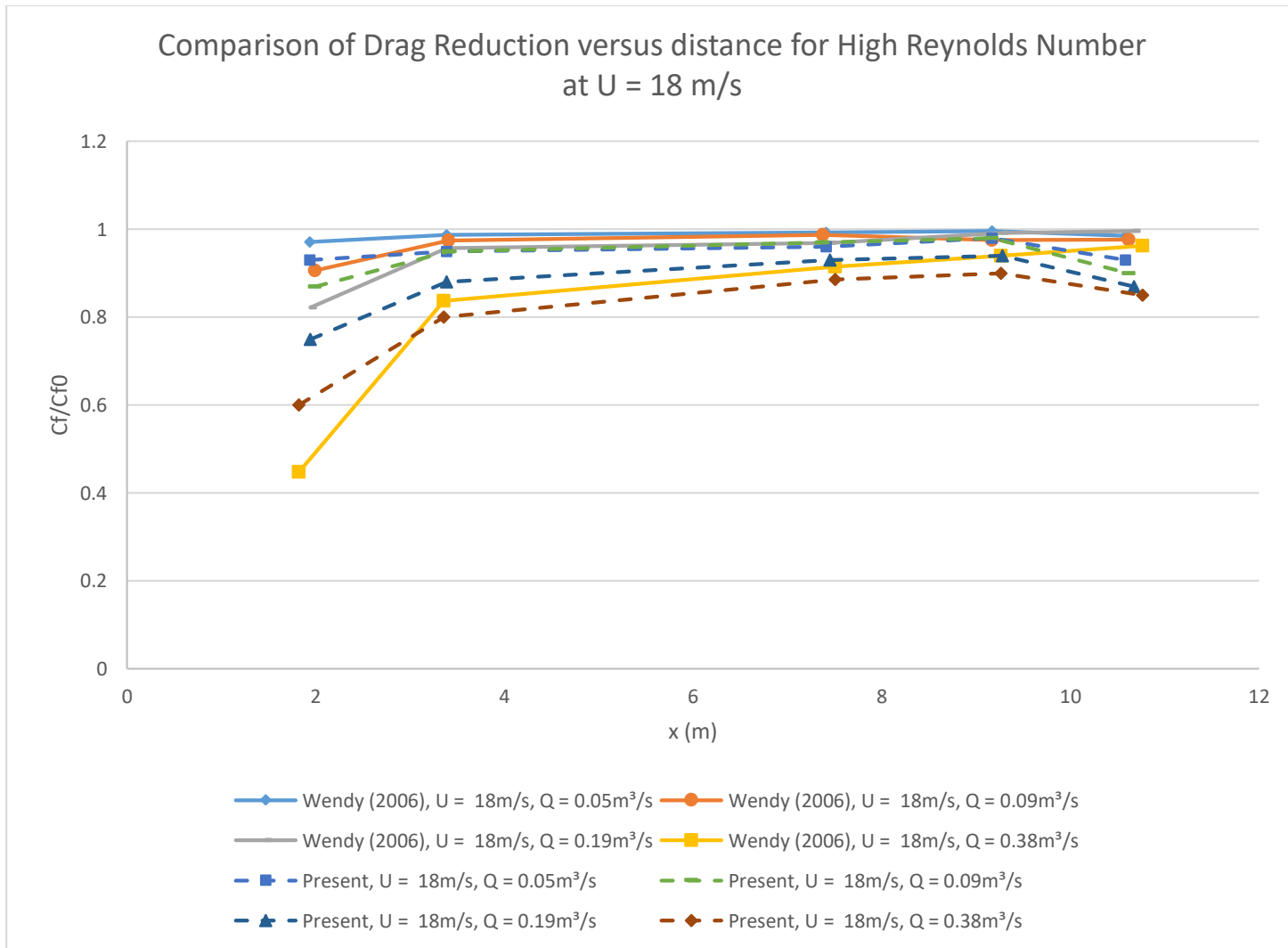


Figure 39: Comparison of Drag Reduction versus distance for High Reynolds Number at  $U = 18 \text{ m/s}$

Figure 39 compares the behavior of the experimental results by Wendy et al. (2006) and present simulations for  $U_\infty = 18 \text{ m/s}$ , while varying values of Q. Both the experimental and simulated results showed that MBDR was indeed distant dependent and showed characteristics similar to the results for  $U_\infty = 12 \text{ m/s}$ . The performance of the MBDR was found to be not as effective as the cases of lower Re. In reality the microbubbles would not be able to create the film surface effectively, similar to the conditions for  $U_\infty = 12 \text{ m/s}$ . Likewise, the performance of MBDR as a function of distance shows that the microbubbles are basically blown away by the flow. It is important to note that increased performance was found for higher flow rates of microbubbles, which validates the fact that MBDR is dependent on the microbubble gas injection rate. There was a good agreement between the simulated and experimental result with the difference being approximately 6%.

## CONCLUSIONS

The modelling of MBDR using ANSYS and comparing the simulated results to experimental data was validated through this thesis. The validation of the model was significant as it can be useful for the prediction and analysis of systems with MBDR. The effect of microbubble drag reduction is applicable over a wide range of applications, even at the verified high Reynolds numbers. For the conditions tested, both by the previous researchers and in this thesis paper, drag reduction was obtained at values of approximately 80-90%. For the cases considered, the two models used to verify the results were; the flat plate by Lin et al (2006) and the other by Wendy et al. (2006). The manner of setting up the system for modelling was used to set up the different plates and conditions and the results obtained were validated. The confirmation of accurate and comparable results deemed method of modelling valid for computing MBDR.

There was a small difference between the experimental results with the CFD analysis, however, the trend lines and general expected trends were similar. The difference can be due to the solver using the Stokes hypothesis of taking the bulk coefficient of viscosity as zero, giving a factor of  $-\frac{2}{3}$  in the momentum conservation equations. There is experimental data which shows that this factor should be approximately three times this order of magnitude, e.g. approximately 1000 for CO<sub>2</sub>. This can be a potential source of the difference in the result. It is recommended that this factor should be determined experimentally and then included in the model.

While the mass fraction average for pure species was used for the calculation of the mixture viscosity there are other methods which could be used to calculate the mixture viscosity. Additionally, the mass source in the first layer of cells to model the microbubbles needs to be properly taken into consideration. For the purpose of the study, I believe that there should be better considered for the modelling. The mass source and sinks terms for the continuity and momentum equations were not used for the purpose of the study but can potentially reduce difference between the experimental and simulated results.

There was strong evidence that the MBDR effectiveness increases with increased bubble flow rate  $Q/U_A$ . The MBDR effectiveness increases rapidly up to a certain value, then becomes almost constant despite the increase of the bubble injection flow rate. The strong effect of the density ratio was analyzed and confirmed through the use of different injected gases into the flow over the flat plate. Additional confirmation for the effect of density ratio was through the use of air vs water as the fluid flowing parallel to the plate. In both cases, the effect of the density ratio was as expected based on the understanding of MBDR. It was confirmed that as the density ratio increases, i.e. the lower the comparative density of the injected gas is, the better the effect of the microbubble drag reduction.

The effect of the roughness was analysis by changing the model slightly to incorporate the friction factor into the wall function. The increase in roughness coefficient lead to an improved value of drag reduction effectiveness. It was

important to note that while MBDR effectiveness increased the friction coefficient may be increased. Increasing the inlet turbulent intensity reduced the drag reduction capabilities of the system. This was expected due to the need to keep the bubbles as a coherent film near to the surface. The increased turbulence intensity can cause the bubbles to be moved out of place by the increased turbulent motion of the flow, thereby reducing MBDR effectiveness.

It is my recommendation that there be a secondary validation of the concepts studied in this paper. It would be important to perform experimental studies for the MBDR effectiveness with air vs water as the fluid as well as the effect of turbulent intensity. For future studies I would also recommend studying the flow at extremely low Reynolds numbers to determine the behavior of other flows and the validity of microbubble drag reduction techniques. To perform this there needs to be both experimental and simulated studies to successfully validate the potential results. Furthermore, a useful study would be determining the behavior and validity of MBDR on curved surfaces. Finally, the changes in heat transfer properties due to MBDR should be studied.

## BIBLIOGRAPHY

1. Alexandrou A. Principles of Fluid Mechanics. New Jersey: Prentice Hall, (2001).
2. Altaf, A., Omar, A., Asrar, W. 2014. Review of Passive Drag Reduction Techniques for Bluff Road Vehicles. IIUM Engineering Journal. Vol 15, No 1.
3. ANSYS User Guide. Last Updated; 01/09/2009. Version 12.  
<http://www.afs.enea.it/project/neptunius/docs/fluent/html/ug/node2.htm>
4. Arithmetic and geometric progressions. 2009. [www.mathcenter.ac.uk](http://www.mathcenter.ac.uk)
5. Buresti, G., Iungo, G., Lombardi, G. 2007. Methods for the Drag Reduction of Bluff Bodies and their Application to Heavy Road-Vehicles. Contract between CRF and DIA.
6. Ceccio, S., Mäkiharju, S., Perlin, M. 2012. On the energy economics of air lubrication drag reduction. Inter Journal of Naval Architecture and Ocean Engineering. 2012. Volume 4, pp 412-422
7. Çengel and Cimbala. Turbulent Flat Plate Boundary Layer. Section 10-6.
8. Celik, I. 1999. Introductory Turbulence Modelling. Unpublished Notes. Mechanical and Aerospace Engineering Department, West Virginia University, P.O. Box 6106, Morgantown, WV 26506-6106
9. Cimbala J.M. 2015. Turbulent Flat Plate Boundary Layer. Lecture Notes. Penn State University College of Engineering.  
[http://www.mne.psu.edu/cimbala/me320web\\_Spring\\_2015/pdf/Flat\\_plate\\_turbulent\\_BL.pdf](http://www.mne.psu.edu/cimbala/me320web_Spring_2015/pdf/Flat_plate_turbulent_BL.pdf).
10. Deutsch, S., Fontaine, A.A., Money, M., Petrie, H. 2004. Microbubble drag reduction in rough walled turbulent boundary layers with comparison against polymer drag reduction. Experiments in Fluids. November 2004, Volume 37, Issue 5, pp 731-744

11. Deutsch, S., Fountaine, A. 1992. The effects of the types of gas on the reduction of skin friction drag by microbubble injection. *Experiments in Fluids*. Volume 13, pp 128-136.
12. Deutsch, S., Madavan, N., Merkle, C. 1982. Measurements of Local Skin Friction in a Microbubble Modified Turbulent layer. Office of Naval Research.
13. Dulikravich, G.S. 2014. Intermediate Fluid Mechanics. Unpublished Notes. Department of Mechanical and Materials Engineering, Florida International University.
14. Ferrante, A., Elghobashi, S. 2004. On the physical mechanisms of drag reduction in spatially developing turbulent boundary layer laden with microbubbles. *Journal of Fluid Mechanics*. Vol 503, pp 345-355.
15. Gutierrez, C., Hassan, Y. 2006. Investigation of Drag Reduction mechanism by Microbubble injection within a channel boundary layer using particle tracking velocimetry. *Nuclear Engineering and Technology*. Volume 38. No 8.
16. Gutierrez, C., Hassan, Y., Bernal, J., Barobosa, J. 2008. Drag reduction by microbubble injection in a channel flow. *Revista Mexicana de Fisica*. Voume 54(1), pp 8-14.
17. Hama FR. "Boundary-layer Characteristics for Rough and Smooth Surfaces." *Trans SNAME* 62: 333-351 (1954).
18. Hashima, A., Yaakob, O., Koh, K, Ismail, N., Ahmed, Y. 2015. Review of Micro-bubble Ship Resistance Reduction Methods and the Mechanisms that Affect the Skin Friction on Drag Reduction from 1999 to 2015. *Jurnal Teknologi*, Volume 74(5), pp 105-114.
19. Hashin, A., Yaakob, O.B., Koh, K.K., Ismail, N., Ahmed, Y.M. 2015. Review of micro-bubble ship resistance reduction methods and the mechanisms that affect the skin friction on drag reduction from 1999 to 2015. *Jurnal Teknologi*. Vol 74, Issue 5, pp 105-114.
20. Hassan, Y. A., 2004. Drag Reduction via Microbubble Injection in Boundary Layer of Channel Flows. In: *Advances in the Modeling Methodologies of Two-Phase Flows Meeting (SHF/IAHR)*, Lyons, France, November 24-26, 2004 and published in the conference proceedings, paper: 08, 2004.

21. Hassan, Y. A., Ortiz-Villafuerte, J., 2002. Experimental study of micro-bubble drag reduction using particle image velocimetry. In 11th International Symposium on Applications of Laser Techniques to Fluid Mechanics 23 (2).
22. Hassan, Y., Orti, J. 2002. Experimental Study of Micro-bubble Drag Reduction Using Particle Image Velocimetry. Department of Nuclear Engineering Texas A&M University. MS 3133.
23. Kodama Y., Kakugawa A., Takahashi T., Nagaya S., Kawamura T., 2013. Drag Reduction of Ships by Microbubbles. National Maritime Research Institute of Japan.
24. Kodama, Y., Sugiyama, K., Makimo, M., Takahashi, T. 2003. The Degree and the Mechanism of Skin Friction Reduction by Microbubbles. Proceedings of Turbulence and Shear Flow Phenomena Conferences. Vol 3 (953).
25. Kunz, R.F., Deutsch, S., Lindau, J.W., 2003. Two fluid modeling of microbubble turbulent drag reduction. In: 4th ASME–JSME Joint Fluids Engineering Conference, Honolulu, Hawaii, July 6–11, 2003, Paper FED2003-45640.
26. Lin, C.X., Skudarnov, P.V. 2005. Density Ratio and Turbulence Intensity Effects in Microbubble Drag Reduction Phenomenon. 2005 ASME Fluids Engineering Division Summer Meeting and Exhibition, June 19-23, 2005, Houston, TX, USA.
27. Lin, C.X., Skudarnov, P.V. 2006. Drag reduction by gas injection into turbulent boundary layer: Density ratio effect. International Journal of Heat and Fluid Flow 27 (2006), 436–444.
28. Lu, J., Fernández, A., Tryggvason, G. 2005. The effect of bubbles on the wall drag in a turbulent channel flow. Physics of Fluids. Vol 17.
29. Madavan, N.K., Deutsch, S., Merkle, C.L. 1984. Reduction of Turbulent Skin Friction by Microbubbles. Physics of Fluids. Vol 27, pp 356-363.
30. Madavan, N.K., Deutsch, S., Merkle, C.L. 1985. Measurements of local skin friction in a microbubble-modified turbulent boundary layer. Journal of Fluid Mechanics. Vol 156, pp 237-256.
31. MENTER, F. 1992. Influence of freestream values on k-omega turbulence model predictions. AIAA Journal, Vol. 30, No. 6, pp. 1657-1659.

32. Merkle, C. 1983. Reduction of Turbulent Skin Friction by Microbubbles. DOI: 10.1063/1.864620
33. Merkle, C.L., Deutsch, S., 1992. Microbubble drag reduction in liquid turbulent boundary layers. *Applied Mechanics Reviews* 45 (3), 103–127.
34. Moody, L. F. 1944. Friction factors for pipe flow. *Transactions of the ASME* 66 (8): 671–684
35. Nikuradse, J. 1933 *Stromungsgesetze in rauhen Rohren*. Forschungshefte 361. VDI, Berlin. Translated in NACA technical memorandum 1292 (1950).
36. Nouri, N., Sarreshtehdari, A., Maghsouchi, E. 2008. Experimental Study of Gas Injection Effect as a Secondary Phase Flow Induced Rotary Hub. *Journal of Applied Sciences*. Volume 8 (11). 2091-2097.
37. Pal, S., Merkle, C., Deutsch, S. 1988. Bubble characteristics and trajectories in a microbubble boundary layer. *Physics of Fluids*. Vol 31, pp 744-751.
38. Pamadi, B., Taylor, L., Leary, T. 1990. A Method for the Reduction of Aerodynamic Drag of Road Vehicles. NASA Technical Memorandum 102589.
39. Pandian, N. 2013. Drag Reduction: The Pursuit of Better Fuel Economy. *Illumin*. University of Southern California. Vol. 14, Issue 1.
40. Patel, V. 1998. Perspective: Flow at High Reynolds Number and Over Rough Surfaces – Achilles Heel of CFD. *Journal of Fluids Engineering*. Volume 120(3), pp 434-444.
41. Raymer, D. 1992. *Aircraft Design a Conceptual Approach*. American Institute of Aeronautics and Astronautics, Inc., Washington, DC. 2<sup>nd</sup> Edition.
42. Rohatgi, U. 2012. Methods of Reducing Vehicle Aerodynamic Drag. Presented at the ASME 2012 Summer Heat Transfer Conference. US Department of Energy.
43. Sayyaadi, H., Nematollahi, M. 2013. Determination of optimum injection flow rate to achieve maximum micro bubble drag reduction in ships; an experimental approach. Center of Excellence in Hydrodynamics and Dynamics of Marine Vehicles, School of Mechanical Engineering, Sharif

University of Technology, Tehran, P.O. Box 11155-9567, Iran Received 11 July 2012; revised 25 December 2012; accepted 8 January 2013.

44. Sayyaadi, H., Nematollahi, M., 2013. Determination of optimum injection flow rate to achieve maximum micro bubble drag reduction in ships; an experimental approach. *Scientia Iranica B* 20 (3), 535–541.
45. Shapiro, A., 2004. The Effect of Surface Roughness on Hydrodynamic Drag and Turbulence. USNA Trident Scholar Report. No 37.
46. Shapiro, T. 2004. The Effect of Surface Roughness on Hydrodynamic Drag and Turbulence. USNA---Trident Scholar project report; no. 327.
47. Sonin, A. A. 2001. Equation of Motion of Viscous Fluids. Department of Mechanical Engineering, Massachusetts Institute of Technology, Cambridge, Massachusetts, 02139. 8<sup>th</sup> Edition.
48. Tritton, D. J. 1998. *Physical Fluid Dynamics*. Oxford University Press, Oxford, England. 2<sup>nd</sup> edition.
49. Truesdell, C. 1954. The present status of the controversy regarding the bulk viscosity of fluids. *Proceedings of the Royal Society of London, Series A. Mathematical and the Physical Sciences*. Volume 226, pp 583-592.
50. Trygvason, G. 2005. The Effect of Bubbles on the Wall Drag in Turbulent Channel Flow.
51. Tsai, J., Chen, C. 2011. Boundary Layer Mixture Model for a Microbubble Drag Reduction Technique. *ISRN Mechanical Engineering*. Volume 2011, Article ID 405701, 9 pages.
52. Vijiapurapu, S., Cui, J. 2010. Performance of turbulence models for flows through rough pipes. *Applied Mathematical Modelling*. Volume 34. pp 1458–1466.
53. Von Karman, Theodore. 1934. Turbulence and Skin Friction. *Journal of the Aeronautical Sciences*. Vol. 1, No 1, pp. 1-20.
54. Washburn, T. 2010. Airframe Drag/Weight Reduction Techniques. Green Aviation Summit. Fuel Burn Reduction. NASA Ames Center.

55. Wendy, S., Winkel, E., Dowling, D., Perlin, M., Ceccio, S. 2006. Bubble friction drag reduction in a high-Reynolds-number flat-plate turbulent boundary layer. *Journal of Fluid Mechanics*. Vol. 552, pp. 353–380.
56. White, FM. 1974 *Viscous fluid flow*. McGraw-Hill, New York, pp 490–491
57. Xie, X. P., Cao, L.F., Zeng, J.H. 2015. Theoretical investigation into friction resistance calculation of van body surface in the presence of air film. *Journal of South China University of Technology (Natural Science)*. Volume 43, Issue 2, pp 96-101.